

The Density Matrix Renormalization Group Method applied to Interaction Round a Face Hamiltonians

Germán Sierra¹ and Tomotoshi Nishino²

¹ Instituto de Matemáticas y Física Fundamental,
C.S.I.C., Madrid, Spain

² Department of Physics, Faculty of Science,
Kobe University, Rokkoudai, Kobe, Japan

October 1996

Abstract

Given a Hamiltonian with a continuous symmetry one can generally factorize that symmetry and consider the dynamics on invariant Hilbert Spaces. In Statistical Mechanics this procedure is known as the vertex-IRF map, and in certain cases, like rotational invariant Hamiltonians, can be implemented via group theoretical techniques. Using this map we translate the DMRG method, which applies to 1d vertex Hamiltonians, into a formulation adequate to study IRF Hamiltonians. The advantage of the IRF formulation of the DMRG method (we name it IRF-DMRG), is that the dimensions of the Hilbert Spaces involved in numerical computations are smaller than in the vertex-DMRG, since the degeneracy due to the symmetry has been eliminated. The IRF-DMRG admits a natural and geometric formulation in terms of the paths or string algebras used in Exactly Integrable Systems and Conformal Field Theory. We illustrate the IRF-DMRG method with the study of the SOS model which corresponds to the spin 1/2 Heisenberg chain and the RSOS models with Coxeter diagram of type A, which correspond to the quantum group invariant XXZ chain.

PACS numbers: 05.50.+q, 11.10.Gh, 75.10.Jm

Introduction

The Density Matrix Renormalization Group is a powerful numerical real space RG method introduced by White in 1992 to study quantum lattice Hamiltonians of interest in Condensed Matter and Statistical Physics [1]. This method has its roots in Wilson's solution of the Kondo problem [2], but it is not confined to impurity problems. The DMRG method overcomes the problems of the old Block RG method of the SLAC [3] and Paris groups [4], which in many cases gives qualitative correct results but lacks numerical accuracy (for a review of the Block RG method see [5, 6]). The DMRG is well suited for 1d problems as spin chains [7, 8] , but it has also been applied successfully to ladder systems [9] and large 2d blocks [10]. Another related developments are : Generalization of the DMRG to classical systems and its relation with the Baxter's Corner Transfer Matrix [11], Variational Formulation of the DMRG ground state wave function [12], Momentum space DMRG [13], application of the DMRG to transfer matrices [14], DMRG study of quantum systems at finite temperature [15], analytic formulation of the DMRG [16]. The correlation between blocks inherent to the DMRG method has also been implemented in the old Block RG method in references [17, 18, 19], etc.

The purpose of this paper is to generalize the DMRG to a class of models commonly known in Statistical Mechanics as Interaction Round a Face (IRF) or more simply Face models [20]. In these models the lattice variables are labelled by the points (heights) of a graph \mathcal{G} , and such that heights located at nearby sites on the lattice must also be nearest neighbours on the graph. The SOS models and the RSOS models, which are a restricted class on the former ones are the most interesting examples of IRF models, due to their connection with Integrable Models [20, 21], Affine Lie algebras [22], Towers of Multi-Matrix Algebras [23, 24] and Conformal Field Theories (CFT) [25]. Other important class of models is given by the vertex models, where the nearby lattice variables are independent, although the Boltzmann weights may satisfy certain conservation laws [26]. The well known Heisenberg, t-J and Hubbard models, are Hamiltonian or transfer matrix versions of vertex models, which can be studied using the DMRG. It is for the later class of theories that applies the standard DMRG. We shall propose in this paper to translate the "vertex language", which is used to formulate the DMRG, into "IRF language". This translation process is suggested by the fact that some models, like the Baxter's 8 vertex, can be mapped into IRF models [27, 28, 29]. Moreover, if the vertex Hamiltonian has a symmetry described by some group (or quantum group), then the vertex-IRF map consists in the factorization of that symmetry. In symbolical terms we may write,

$$\text{IRF} = \frac{\text{Vertex}}{\text{Symmetry}} \quad (1)$$

In the case of the Heisenberg model, the factorization of the rotational symmetry has lead us to formulate the DMRG in IRF variables. The vertex-IRF map is given in this example by the tensor product decomposition of irreps of $SU(2)$. The heights coincide with the irreps of this group. From (1) it is clear that an advantage in working with IRF variables is that the symmetry present in the vertex Hamiltonian is factorized, and consequently the dimension of the Hilbert spaces involved is much lower. For numerical purposes this property is also important since it implies a reduction of the computational complexity of the problem. On the other hand the IRF formulation of the DMRG is the most natural one to discuss its relation with the corner transfer matrix formalism and CFT.

The organization of the paper is as follows. In section I we review the basic concepts and

tools of the IRF models. In section II we introduce the real space renormalization group method applied to IRF Hamiltonians. In section III we define the density matrix for IRF states and use it to propose the IRF-DMRG algorithm. In section IV we apply the IRF-DMRG to the SOS model, which corresponds to the spin 1/2 Heisenberg model, and to the RSOS models whose graph is a Coxeter diagram of type A, and which are related to the minimal models of Belavin, Polyakov and Zamolodchikov [30]. In section V we describe the vertex-IRF map for Hamiltonians with spin rotation symmetry, and derive the IRF-DMRG from the vertex-DMRG. Finally we state our conclusions and prospects.

I) IRF Models : Basics

The IRF models were introduced by Baxter [20] as Statistical Mechanical models where the variables are defined on the vertices of the square lattice while the interactions are defined on the faces. These kind of models should be distinguished from the vertex ones, where the variables are located on the edges and the interaction is defined on the vertices where four edges meet [26]. In certain cases there will be a deep relationship between these two types of models, given by a vertex-IRF map. The most interesting class of IRF models are the so called graph-IRF models (for a review see [31]). The heights of these models are labelled by the vertices of a graph \mathcal{G} . The allowed configurations are restricted by the constraint that the lattice variables that are nearest neighbour in the lattice are also nearest neighbour in the graph \mathcal{G} . A characterization of \mathcal{G} is given by its incidence matrix $\Lambda_{a,b}$ which is 1 (resp. 0) if the heights a and b are connected (resp. disconnected) by a link of \mathcal{G} . We assume that there is at most one link connecting any two points. The graphs which we shall study in this paper are bipartite, which means that they can be partitioned into two subgraphs, say even and odd, so that any point of one subgraph is connected only to points of the other subgraph. A pair of variables (a, b) is said to be admissible if $\Lambda_{a,b} = 1$. In this terminology, all the heights connected by a link of the square lattice must be admissible. An important example of IRF models are the RSOS models for which \mathcal{G} is a ADE Coxeter diagram, which will be studied in detail in section IV. The A_r graph consists of r points labelled by $a = 1, 2, \dots, r$.

In the Hamiltonian or transfer matrix formulation of IRF models, a state of the Hilbert space is described by the ket,

$$|\mathbf{a}\rangle = |a_0, a_1, \dots, a_N\rangle \quad (2)$$

where (a_i, a_{i+1}) is an admissible pair. There is a geometrical interpretation of the IRF states as paths on a Bratelli diagram, which is constructed by folding the graph as in figure 1, and repeating the pattern along the "x-axis" [23, 32]. A path ξ on the Bratelli diagram is a succession of points $\{\xi(i)\}_{i=0}^N$ such that the couple $(\xi(i), \xi(i+1))$ coincides with a link of the diagram (see figure 2). Another important concept is that of a plaquette on the Bratelli diagram. A plaquette is the four-tuple,

$$(a, b, c, d) \equiv \begin{pmatrix} & d & \\ a & & c \\ & b & \end{pmatrix}, \quad (a, b), (b, c), (a, d), (d, c) : \text{admissible} \quad (3)$$

and can be identified with the elementary squares or plaquettes of the Bratelli diagram.

The IRF models can be defined on periodic or open chains. In this paper we shall concentrate on the later case. To define the dynamics of the IRF model we shall introduce the plaquette operator X_i , which gives the infinitesimal evolution of an IRF state in the neighbourhood of the i^{th} -site of the chain,

$$X_i | \dots, a_{i-1}, a_i, a_{i+1}, \dots \rangle = \sum_{a'_i} R \left(\begin{array}{ccc} & a'_i & \\ a_{i-1} & & a_{i+1} \\ & a_i & \end{array} \right) | \dots, a_{i-1}, a'_i, a_{i+1}, \dots \rangle \quad (4)$$

$R(a_{i-1}, a_i, a_{i+1}, a'_i)$ denotes the local Hamiltonian associated to the plaquette $(a_{i-1}, a_i, a_{i+1}, a'_i)$. If $R(a_{i-1}, a_i, a_{i+1}, a'_i)$ is replaced by a Boltzmann weight then the operators X_i are those introduced by Baxter in the study of integrable IRF models. In our case we are working with infinitesimal versions of these Boltzmann weights and, on the other hand we do not need to impose any kind of integrability condition, although it could be interesting to analyze a possible interplay between the RG and integrability.

The Hamiltonian acting on an open chain is defined as,

$$H = \sum_{i=1}^{N-1} X_i \quad (5)$$

The time evolution produced by (5) preserves the boundary heights $a = a_0$ and $b = a_N$. We shall call $\mathcal{H}_{a,b}^N$ the Hilbert space expanded by IRF states with these boundary conditions,

$$\mathcal{H}_{a,b}^N = \{ |a_0, a_1, \dots, a_N \rangle \mid a_0 = a, a_N = b \} \quad (6)$$

Below we shall consider a generalization of this type of Hilbert spaces characterized by fixed boundary conditions at the ends.

To finish this section we shall review other applications of IRF ideas in the context of Particle Physics, which will help us to introduce new concepts in the next section.

It is well known the connection between integrable statistical models and factorizable S-matrix theories [33]. For example, the Boltzmann weights of the 6 vertex model can be conveniently identified with the scattering S-matrix of the solitons of the sine-Gordon theory. This kind of interpretation is also possible for IRF-Boltzmann weights, which may describe the S-matrix of solitons (or kinks) which connect different vacua. A soliton say $S_{a,b}(\theta)$ with rapidity θ , is a field configuration which connects the vacuum a at $x = -\infty$ with the vacuum b at $x = +\infty$. Two solitons say $S_{a,b}(\theta_1)$ and $S_{b,c}(\theta_2)$ can meet at the common vacuum b and after a certain time the middle vacuum b can turn into a new vacuum, say d . The corresponding S matrix for the process $S_{a,b}(\theta_1)S_{b,c}(\theta_2) \rightarrow S_{a,d}(\theta_2)S_{d,c}(\theta_1)$ is described by the Boltzmann weight associated to the plaquette (3) and rapidity $\theta_1 - \theta_2$. In this terminology the IRF state (2) can be interpreted as a collective state formed by N solitons connecting the vacuum a_0 and a_N through a series of interpolating vacua a_1, \dots, a_{N-1} .

There is yet another interpretation of the IRF states. If we view the graph \mathcal{G} as the target space of a discretized string, then (2) becomes the state of an open string $S_{a,b}$ with fixed boundary conditions at the ends. As in the case of solitons, the strings may join and split in various ways according to graph rules. In the rest of the paper we shall consider as equivalent the interpretations of the IRF states as paths on a Bratteli diagram, kinks of a field theory and discrete strings (see figure 3),

$$\text{Path} = \text{Kink} = \text{String} \tag{7}$$

II) RG of IRF-Hamiltonians: Generalities

The basic problem we want to address is the construction of the ground state and excited states of the IRF Hamiltonian (5) for large values of N . The RG method gives an approximate answer to this difficult problem. Wilson's strategy for the Kondo problem is to start out from small chains and grow them by adding site by site, while keeping a fixed, and usually large number of states, say m , as "representatives" of the whole chain. This method is known as the onion scheme, to be distinguished from the Wilson-Kadanoff blocking scheme which consists in the partition of the chain, or more generally the lattice, into blocks which are afterwards renormalized getting smaller lattices.

The Wilsonian growth process applied to an IRF state is depicted in figure 4. A string (kink) with states $*$ and a and its ends, "absorbs" a particle (vacuum) in a state b becoming a new string (kink) with BC's $(*, b)$. Of course the pair (a, b) should be admissible for the absorption process to be possible. The state $*$ at the l.h.s. of the string will be kept fixed in the construction of "longer" strings. The strings will grow from their r.h.s.

String Hilbert Spaces

Let us call $\mathcal{H}_{*,a}^S$, or more simply \mathcal{H}_a^S , the Hilbert space of the strings S which have BC's $*, a$ at their ends. An example of \mathcal{H}_a^S is given by the Hilbert space (6), where N measures the length of the string S . The RG method will lead to the construction of Hilbert spaces \mathcal{H}_a^S which are imbedded into \mathcal{H}_a^N for some N .

The Hilbert space of the string S with an added point \bullet on its r.h.s. will be denoted by $\mathcal{H}_a^{S\bullet}$ and it is given by,

$$\mathcal{H}_a^{S\bullet} = \bigoplus_{b|\Lambda_{a,b}=1} \mathcal{H}_b^S \tag{8}$$

which implies,

$$\dim \mathcal{H}_a^{S\bullet} = \sum_b \Lambda_{a,b} \dim \mathcal{H}_b^S \tag{9}$$

Proceeding as above one can construct longer strings as for example $S\bullet\bullet$. All what is needed is the "fusion" matrix Λ . For later convenience we give below the basis of the most common string spaces,

$$\begin{aligned} \mathcal{H}_a^S &= \{|\xi_a \rangle\} \\ \mathcal{H}_b^{S\bullet} &= \{|\xi_a \otimes b \rangle \mid \Lambda_{a,b} = 1\} \\ \mathcal{H}_c^{S\bullet\bullet} &= \{|\xi_a \otimes b \otimes c \rangle \mid \Lambda_{a,b} = \Lambda_{b,c} = 1\} \\ &\vdots \end{aligned} \tag{10}$$

A generic Hilbert space of the form $\mathcal{H}^{S\bullet\cdots\bullet}$ will be denoted by $\mathcal{H}_a^{S,n\bullet}$. The complete Hilbert space of a string S plus n points \bullet , consists in the direct sum,

$$\mathcal{H}^{S,n\bullet} = \oplus_a \mathcal{H}_a^{S,n\bullet} \quad (11)$$

The total dimension of $\mathcal{H}^{S,n\bullet}$ can be computed from eq.(9),

$$m_{S,n\bullet} \equiv \dim \mathcal{H}^{S,n\bullet} = \sum_{a_0, \dots, a_n} \Lambda_{a_0, a_1} \dots \Lambda_{a_{n-1}, a_n} m_{a_n} \quad (12)$$

where $m_a = \dim \mathcal{H}_a^S$. It is important to realize that the sum over heights in (12) may not contain all the heights of the graph. For example for a bipartite graph only even or odd heights will appear at the right end of the string (in this sense the strings associated to a bipartite lattice can be classified as even or odd). Thus if the string S is even (odd) the string plus one point $S\bullet$ will be odd (even), and $S\bullet\bullet$ will again be even (odd), etc.

String Operators

We shall call string operators those operators $\mathcal{O}^{S,n\bullet}$ which acting on the Hilbert space $\mathcal{H}^{S,n\bullet}$, do not change the height located at right hand end of the combined system $S\bullet \cdot^n \bullet$. Their action on the basis (10) is given as follows,

$$\begin{aligned} \mathcal{O}^S |\xi_a \rangle &= \sum_{\xi'_a} |\xi'_a \rangle \langle \xi'_a | \mathcal{O}^S |\xi_a \rangle \\ \mathcal{O}^{S\bullet} |\xi_a \otimes b \rangle &= \sum_c \sum_{\xi'_c} |\xi'_c \otimes b \rangle \langle \xi'_c \otimes b | \mathcal{O}^{S\bullet} |\xi_a \otimes b \rangle \\ \mathcal{O}^{S\bullet\bullet} |\xi_a \otimes b \otimes c \rangle &= \sum_{d,e} \sum_{\xi'_e} |\xi'_e \otimes d \otimes c \rangle \langle \xi'_e \otimes d \otimes c | \mathcal{O}^{S\bullet\bullet} |\xi_a \otimes b \otimes c \rangle \\ &\vdots \end{aligned} \quad (13)$$

The matrix elements of the operators $\mathcal{O}^{S,n\bullet}$ appearing in (13) will be denoted by,

$$\begin{aligned} \langle \xi'_a | \mathcal{O}^S |\xi_a \rangle &= \mathcal{O}_{\xi'_a}^{\xi'_a} (*a) \\ \langle \xi'_c \otimes b | \mathcal{O}^{S\bullet} |\xi_a \otimes b \rangle &= \mathcal{O}_{\xi'_c}^{\xi'_c} \begin{pmatrix} c & & \\ * & b & \\ & a & \end{pmatrix} \\ \langle \xi'_e \otimes d \otimes c | \mathcal{O}^{S\bullet\bullet} |\xi_a \otimes b \otimes c \rangle &= \mathcal{O}_{\xi'_e}^{\xi'_e} \begin{pmatrix} & e & d & \\ * & & & c \\ & a & b & \end{pmatrix} \\ &\vdots \end{aligned} \quad (14)$$

and can be depicted as $2(n+1)$ -gons, with a special vertex $*$ from which emanate two thick lines representing string states labelled by ξ (see figure 5). The remaining $2n$ thin lines connect admissible pairs of heights. The most important examples of string operators are given by the Hamiltonians $H^{S,n\bullet}$. However not all the string Hamiltonians are independent. Actually, given $H^{S\bullet}$ and the "Boltzmann weight" R (4) one can build up the remaining Hamiltonians $H^{S,n\bullet}$ for $n \geq 2$. The first member of the later family, namely H^S , has to be given independently, but quite paradoxically it plays little role in the construction.

As an example we give below the matrix representation of $H^{S\bullet\bullet}$,

$$\begin{aligned}
& H_{\xi_a}^{\xi'_e} \begin{pmatrix} e & d \\ * & c \\ a & b \end{pmatrix} \\
& = H_{\xi_a}^{\xi'_e} \begin{pmatrix} e & \\ * & b \\ a & \end{pmatrix} \delta_{b,d} \Lambda_{b,c} + \delta_{a,e} \delta_{\xi_a, \xi'_e} R \begin{pmatrix} d \\ a & c \\ b \end{pmatrix}
\end{aligned} \tag{15}$$

This eq. is depicted in figure 6, where we show also the construction of $H^{S,3\bullet}$.

The RG-operation

The key point of the RG method is the construction of the RG-operator T that truncates the Hilbert space $\mathcal{H}^{S\bullet}$ into $\mathcal{H}^{S'}$, where S' represents a string with one more site than the string S , i.e.

$$T : \mathcal{H}^{S\bullet} \longrightarrow \mathcal{H}^{S'} \tag{16}$$

The matrix representation of T and its hermitean conjugate T^\dagger are given by,

$$\begin{aligned}
T|\xi_a \otimes b \rangle &= \sum_{\xi'_b} T_{\xi_a}^{\xi'_b} \begin{pmatrix} * & b \\ a & \end{pmatrix} |\xi'_b \rangle \\
T^\dagger|\xi'_b \rangle &= \sum_a \sum_{\xi_a} \bar{T}_{\xi'_b}^{\xi_a} \begin{pmatrix} a \\ * & b \end{pmatrix} |\xi_a \otimes b \rangle
\end{aligned} \tag{17}$$

where

$$\left[T_{\xi_a}^{\xi'_b} \begin{pmatrix} * & b \\ a & \end{pmatrix} \right]^* = \bar{T}_{\xi'_b}^{\xi_a} \begin{pmatrix} a \\ * & b \end{pmatrix} \tag{18}$$

According to (16) T is a $m_{S'} \times m_{S\bullet}$ matrix. Except for the first RG-operations we shall always keep the same number of states describing the renormalized system, i.e. $m = m_S = m_{S'}$. Both T and T^\dagger can be depicted as triangles with the special vertex $*$, which is the origin of two thick edges which symbolize the old and new (renormalized) strings (see figure 7). The truncation operator must satisfy the equation,

$$TT^\dagger = \mathbf{1} \tag{19}$$

which guarantees that $T^\dagger T$ is a projection operator which maps $\mathcal{H}^{S\bullet}$ into a subspace which is isomorphic to $\mathcal{H}^{S'}$.

Eq.(19) reads in components (see figure 8),

$$\sum_a \sum_{\xi_a} T_{\xi_a}^{\xi''_b} \begin{pmatrix} * & b \\ a & \end{pmatrix} \bar{T}_{\xi'_b}^{\xi_a} \begin{pmatrix} a \\ * & b \end{pmatrix} = \delta_{\xi'_b, \xi''_b} \tag{20}$$

Given the operators T and T^\dagger we can renormalized any operator $\mathcal{O}^{S,n\bullet}$ down to an operator $\mathcal{O}^{S',(n-1)\bullet}$ by means of the equation,

$$\mathcal{O}^{S',(n-1)\bullet} = T \mathcal{O}^{S,n\bullet} T^\dagger, \quad (n \geq 1) \quad (21)$$

which in mathematical terms expresses the commutativity of the following diagram,

$$\begin{array}{ccc} \mathcal{H}^{S',(n-1)\bullet} & \xrightarrow{\mathcal{O}^{S',(n-1)\bullet}} & \mathcal{H}^{S',(n-1)\bullet} \\ T^\dagger \downarrow & & \uparrow T \\ \mathcal{H}^{S,n\bullet} & \xrightarrow{\mathcal{O}^{S,n\bullet}} & \mathcal{H}^{S,n\bullet} \end{array} \quad (22)$$

In eqs.(21) and (22) the operators T and T^\dagger act trivially on the points beyond the closest one to the string S . As an example we give below the renormalization of $\mathcal{O}^{S,\bullet}$ and $\mathcal{O}^{S,2\bullet}$ (see figures 9 and 10),

$$\mathcal{O}_\xi^{\xi'}(*, b) = \sum_{a,c,\eta,\eta'} T_{\eta'}^{\xi'} \begin{pmatrix} * & c \\ & b \end{pmatrix} \mathcal{O}_\eta^{\eta'} \begin{pmatrix} c & \\ * & b \\ a & \end{pmatrix} \bar{T}_\xi^\eta \begin{pmatrix} a \\ * & b \end{pmatrix} \quad (23)$$

$$\mathcal{O}'_\xi^{\xi'} \begin{pmatrix} c & \\ * & b \\ a & \end{pmatrix} = \sum_{d,e} \sum_{\eta,\eta'} T_{\eta'}^{\xi'} \begin{pmatrix} * & c \\ & e \end{pmatrix} \mathcal{O}_\eta^{\eta'} \begin{pmatrix} e & c \\ * & b \\ d & a \end{pmatrix} \bar{T}_\xi^\eta \begin{pmatrix} d \\ * & a \end{pmatrix} \quad (24)$$

In summary we have presented in this section a formalism to deal with the renormalization of generic IRF Hamiltonians. In the next section we shall explain the DMRG algorithm to construct the truncation operator T , which will then allow us to carry out explicit computations.

III) The IRF-DMRG algorithm

The "standard" RG method to construct the operator T applied to IRF models consists in the following two steps: i) diagonalization of the Hamiltonian $\mathcal{H}^{S\bullet}$ and ii) projection to its lowest energy states. This algorithm treats the system $S\bullet$ as isolated from the rest of points which one adds in posteriori RG steps. In other words, the height associated to the point \bullet in $S\bullet$ is fixed to a given value. Imposing fixed boundary conditions at the ends of the blocks in the RG method always leads to bad results. Instead one should consider a combination of B.C.'s as in [34], or impose open B.C.'s as in [18].

The DMRG is a way to take care of the influence or correlations of those points that have not yet been added to the block. There are various DMRG algorithms: infinite system method, finite system method, etc. We shall give in this paper the IRF version of the infinite system algorithm, which is based on the superblock formed by a string S , a point \bullet and another string S^R , which is the mirror image or reflection of the string S (see figure 11). The dynamics of the "super-string" $S\bullet S^R$ involves all allowed heights at the middle point \bullet , and in that way one is not committed to a particular B.C. on \bullet . There is an appealing electrostatic analogy to understand the role of S^R . Let us recall the mirror image method which is used to impose Neumann (open) B.C.'s on the electrostatic potential. In this sense the mirror string S^R seems to play a similar role, i.e. that of imposing open B.C.'s on \bullet .

A basis of the Hilbert space of the super-string $S\bullet S^R$ is given by,

$$\mathcal{H}^{S\bullet S^R} = \{|\xi_a \otimes b \otimes \eta_c \rangle \mid \Lambda_{a,b} = \Lambda_{b,c} = 1\} \quad (25)$$

The Hamiltonian which generates the dynamics of the states belonging to $\mathcal{H}^{S\bullet S^R}$ can be obtained using the methods of the last section and it reads (recall figure 6),

$$\begin{aligned} H_{\xi,\eta}^{\xi',\eta'} \begin{pmatrix} & a' & b' & c' \\ * & & & * \\ & a & b & c \\ & & & \end{pmatrix} &= H_{\xi}^{\xi'} \begin{pmatrix} & a' & \\ * & & b \\ & a & \end{pmatrix} \delta_{b,b'} \delta_{c,c'} \Lambda_{b,c} \delta_{\eta,\eta'} \\ + \delta_{a,a'} \delta_{\xi,\xi'} R \begin{pmatrix} & b' & \\ a & & c \\ & b & \end{pmatrix} \delta_{c,c'} \delta_{\eta,\eta'} &+ \delta_{a,a'} \delta_{b,b'} \Lambda_{a,b} \delta_{\xi,\xi'} H_{\eta}^{\eta'} \begin{pmatrix} & c' & \\ * & & b \\ & & c \end{pmatrix} \end{aligned} \quad (26)$$

Now we diagonalize this Hamiltonian and select its ground state which is called the target state and can be written as,

$$|\psi_0 \rangle = \sum_{a,b,c} \sum_{\xi,\eta} \psi_{\xi,\eta}(a,b,c) |\xi \otimes b \otimes \eta \rangle \quad (27)$$

The mirror string S^R plays an auxiliary role in the construction and we should get rid of it. The DMRG proposal is to construct the reduced density matrix $\rho^{S\bullet}$ of the subsystem $S\bullet$ by tracing over the states in S^R ,

$$\rho^{S\bullet} = \text{Tr}_{\mathcal{H}^{S^R}} |\psi_0 \rangle \langle \psi_0| \quad (28)$$

In the above trace we shall set the height of the middle point the same for both the ket and the bras, so that the matrix representation of $\rho^{S\bullet}$ will be given by,

$$\rho_{\xi}^{\xi'} \begin{pmatrix} & a' & \\ * & & b \\ & a & \end{pmatrix} = \sum_c \sum_{\eta} \psi_{\xi,\eta}(a,b,c) \psi_{\xi',\eta}^*(a',b,c) \quad (29)$$

A normalized ground state (27) yields a properly normalized density matrix,

$$\text{Tr}_{\mathcal{H}^{S\bullet}} \rho^{S\bullet} = \sum_{a,b} \sum_{\xi} \rho_{\xi}^{\xi} \begin{pmatrix} & a & \\ * & & b \\ & a & \end{pmatrix} = 1 \quad (30)$$

The next step is to diagonalize the matrix (29) in the Hilbert space $\mathcal{H}_b^{S\bullet}$, for every value of b , keeping the first m eigenstates with highest eigenvalue. These states are the most probable ones to contribute to the ground state of the super-string. Finally the matrix T (16) is given by these m column vectors.

Eq.(29) is very similar to Baxter's definition of the corner transfer matrix (CTM) for IRF models [20], in the sense that one traces over the degrees of freedom of half of the system while keeping the height located at the edge of the "cut" fixed. This relation between the DMRG and the CTM has already been pointed out in [11], and we expect it to hold also for the IRF-DMRG.

This ends our presentation of the IRF-DMRG.

IV) The IRF-DMRG at work

We shall apply below the formalism developed in the last two sections to study IRF models that can be obtained by means of vertex-IRF maps of vertex Hamiltonians. This map will be explained in detail in section V for the case of the SOS models.

SOS model (S=1/2)

The spin chain Hamiltonian of the Heisenberg model with spin 1/2 reads,

$$H = \frac{1}{2} \sum_i (\vec{\sigma}_i \vec{\sigma}_{i+1} + 1) \quad (31)$$

where $\vec{\sigma}_i$ are Pauli matrices acting at the i^{th} site of the chain. The choice of (31) is motivated by the fact that $\frac{1}{2} (\vec{\sigma}_i \vec{\sigma}_{i+1} + 1)$ is the permutation operator acting at the sites i and $i + 1$. The model defined by (31) is equivalent to an IRF model whose graph, denoted by A_∞ , consists in the semi-infinite chain of fig. 12. The heights $j = 0, 1/2, 1, \dots$, that label the points of the graph A_∞ , are in one-to-one correspondence with the irreps of the group $SU(2)$. According to fig. 12 the incidence matrix of A_∞ satisfies

$$\Lambda_{j,j'} = 1 \iff |j - j'| = 1/2 \quad (32)$$

The IRF-Hilbert space associated to a chain with N -sites is given by the direct sum (recall (11)),

$$\mathcal{H}^N = \oplus_j \mathcal{H}_j^N \quad (33)$$

where \mathcal{H}_j^N is the IRF-Hilbert space of all the states with total spin j ,

$$\mathcal{H}_j^N = \{ |j_0, j_1, \dots, j_N \rangle \mid j_0 = 0, j_N = j, |j_i - j_{i+1}| = 1/2 \text{ for } i = 0, \dots, N-1 \} \quad (34)$$

According to (34) the height \star should be identified with the identity irrep (i.e. $\star = 0$). Since the graph A_∞ contains an infinite number of heights this model is an unrestricted IRF model called solid-on-solid model (SOS). This implies in particular that the Bratelli diagram consists of a pyramid of infinite height as one moves from the origin of the diagram (i.e. \star point = vacuum representation) to the right hand side (fig.13).

The dimension of the Hilbert space (34) is given by,

$$\dim \mathcal{H}_j^N = \binom{N}{\frac{N}{2} - j} - \binom{N}{\frac{N}{2} - j - 1} \quad (35)$$

This formula can be compared with the number of vertex states of the standard formulation of the Heisenberg model, with a fixed value of the third component of the spin s^z (see section V) ,

$$\dim \mathcal{V}_{s^z}^N = \binom{N}{\frac{N}{2} - s^z} \quad (36)$$

For N even (odd) the ground state will belong to the Hilbert space with $j = 0$ ($1/2$). As can be seen from eqs.(35) and (36) it is more efficient, for numerical purposes, to look for the ground state of the Heisenberg model in the IRF subspaces than in the vertex ones (see table 1).

N	$\dim \mathcal{H}_{j=0}^N(\text{IRF})$	$\dim \mathcal{H}_{s^z=0}^N(\text{vertex})$
4	2	6
10	42	252
20	16 796	184 756
24	208 012	2 704 156
$N \gg 1$	$\sim 1.59562^N / N^{3/2}$	$\sim 0.79782^N / N^{1/2}$

Table 1

From (35) and (36) we get the relation,

$$\frac{\dim \mathcal{V}_{s^z=0}^N}{\dim \mathcal{H}_{j=0}^N} = \frac{N}{2} + 1 \quad (37)$$

which is a numerical version of the eq.(1) and shows that the difference between the vertex and IRF formulations persists in the thermodynamic limit.

The constraints (32) imply that there are only 6 different "Boltzmann" weights whose values are given in table 2.

$\begin{matrix} & d & \\ a & & c \\ & b & \end{matrix}$	$R \begin{pmatrix} & d & \\ a & & c \\ & b & \end{pmatrix}$
$\begin{matrix} & j & \\ j \pm 1/2 & & j \mp 1/2 \\ & j & \end{matrix}$	1
$\begin{matrix} & j \pm 1/2 & \\ j & & j \\ & j \pm 1/2 & \end{matrix}$	$\frac{\mp 1}{2j+1}$
$\begin{matrix} & j \pm 1/2 & \\ j & & j \\ & j \mp 1/2 & \end{matrix}$	$\frac{\sqrt{2j(2j+2)}}{2j+1}$

Table 2: The SOS (S=1/2) Hamiltonian.

Numerical Results

In table 3 we present the data for the ground state energy of the Heisenberg Hamiltonian (31) for chains of length $N = 6$ up to 24. In this IRF-DMRG computation we keep $m=12$ states, which is a rather modest number of states, while for the vertex-DMRG we keep a maximum of 12 states, since it is impossible to fix the number of m for vertex-DMRG, due to the degeneracy based on $SU(2)$ symmetry. This is one of the advantages of the IRF-DMRG as compared with the vertex-DMRG. It is clear that at equal number of retained states, the IRF method should give better results than the vertex method. This expectation is confirmed in table 3.

N	Exact	IRF-DMRG	Vertex DMRG
6	-2.4871542677758	-2.4871542677758 *	-2.4871542677758 *
8	-3.2498651973757	-3.2498651973757 *	-3.2498651973757 *
10	-4.0160704145657	-4.0160704145657 *	-4.0160641768009
12	-4.7841812656810	-4.7841812656810 *	-4.7835746471807
14	-5.5534493237243	-5.5534493236562	-5.5527041895949
16	-6.3234742911502	-6.3234742887647	-6.3246392674964
18	-7.0940221370730	-7.0940221268443	-7.0953356164320
20	-7.8649466687979	-7.8649466378157	-7.8663701424885
22	-8.6361517519671	-8.6361516790424	-8.6375643759289
24	-9.4075715208191	-9.4075713713902	-9.4089821742785

Table 3: Ground state energy of the Hamiltonian (31). The data followed by "*" are exact.

If we increase the number m of states retained, the results converge exponentially fast both in the vertex-DMRG and IRF-DMRG methods (fig.14).

RSOS models

An interesting generalization of the spin 1/2 Heisenberg chain is provided by the XXZ Hamiltonian with boundary terms [35] ,

$$H^{XXZ} = \frac{1}{2} \left[\sum_{i=1}^{N-1} \left(\sigma_i^X \sigma_{i+1}^X + \sigma_i^Y \sigma_{i+1}^Y + \frac{q + q^{-1}}{2} \sigma_i^Z \sigma_{i+1}^Z \right) + \frac{q - q^{-1}}{2} (\sigma_1^Z - \sigma_N^Z) \right] \quad (38)$$

where $q = e^{i\gamma}$ is a phase. This Hamiltonian has very interesting properties:

- The eigenenergies of the N=2M site XXZ chain (38) coincide with those a M-site self-dual Q-state Potts model with $Q = q + q^{-1} = 2 \cos\gamma$ [36, 37].
- Invariance under the action of the quantum group $SU(2)_q$ [38].
- Using q-group theory one can map the vertex Hamiltonian (38) into a RSOS Hamiltonian whose graph is given by the Coxeter diagram A_r (see figure 15) [29].
- H^{XXZ} is critical [35] and for $\gamma = \frac{\pi}{r+1}$ it belongs to the universality class of the minimal CFT's [30] with a value of the central charge given by,

$$c = 1 - \frac{6}{r(r+1)} \quad (39)$$

We shall study below the RSOS version of the vertex Hamiltonian (38). A way to arrive to this version consists in writing (38) as follows [39] ,

$$H^{XXZ} = \sum_{i=1}^{N-1} \left(\frac{q+q^{-1}}{4} - e_i \right) \quad (40)$$

where e_i are the Temperley-Lieb-Jones (TLJ) operators which act at the positions i^{th} and $(i+1)^{th}$ of the chain and satisfy the TLJ algebra [31],

$$\begin{aligned}
e_i^2 &= (q + q^{-1})e_i \\
e_i e_{i\pm 1} e_i &= e_i \\
e_i e_j &= e_j e_i, \quad |i - j| \geq 2
\end{aligned} \tag{41}$$

In the vertex basis the TLJ operator e_i can be written as follows,

$$e_i = \mathbf{1}_1 \otimes \cdots \otimes \mathbf{1}_{i-1} \otimes \begin{pmatrix} 0 & 0 & 0 & 0 \\ 0 & q^{-1} & -1 & 0 \\ 0 & -1 & q & 0 \\ 0 & 0 & 0 & 0 \end{pmatrix} \otimes \mathbf{1}_{i+2} \cdots \otimes \mathbf{1}_N \tag{42}$$

The existence of a vertex-IRF map, and the fact that the operators e_i commute with the action of $SU(2)_q$ imply that they can be given a representation on the RSOS-Hilbert spaces of the face model defined by the graph A_r ,

$$e_i | \dots, a_{i-1}, a_i, a_{i+1}, \dots \rangle = \sum_{a'_i} e \begin{pmatrix} & a'_i & \\ a_{i-1} & & a_{i+1} \\ & a_i & \end{pmatrix} | \dots, a_{i-1}, a'_i, a_{i+1}, \dots \rangle \tag{43}$$

$$e \begin{pmatrix} & d & \\ a & & c \\ & b & \end{pmatrix} = \delta_{a,c} \frac{\sqrt{t_b t_d}}{t_a} \tag{44}$$

where t_a are the components of the Perron-Frobenius vector of the incidence matrix of the graph A_r , which are given by

$$t_a = \sin \left(\frac{\pi a}{r+1} \right), \quad a = 1, 2, \dots, r \tag{45}$$

Notice that t_a satisfies,

$$t_{a+1} + t_{a-1} = 2 \cos \left(\frac{\pi}{r+1} \right) t_a \tag{46}$$

Recalling that the incidence matrix satisfies in this case

$$\Lambda_{a,b} = 1 \iff |a - b| = 1 \tag{47}$$

one gets that there are only 6 types of "Boltzmann weights", whose expression, given in table 4, can be computed using eqs (40) and (44),

d $a \quad c$ b	$R \begin{pmatrix} d & \\ a & c \\ & b \end{pmatrix}$
a $a \pm 1 \quad a \mp 1$ a	$\frac{\cos \gamma}{2}$
$a \pm 1$ $a \quad a$ $a \pm 1$	$\frac{\cos \gamma}{2} - \frac{t_{a+1}}{t_a}$
$a \pm 1$ $a \quad a$ $a \mp 1$	$-\frac{\sqrt{t_{a+1}t_{a-1}}}{t_a}$

Table 4: The RSOS Hamiltonian for the face model A_r .

In the limit where $r \rightarrow \infty$ the RSOS model A_r becomes equivalent to the SOS model with graph A_∞ studied previously. One can check that the R-matrix given in table 4 is, up to a constant and a change of basis, the same as the R-matrix given in table 2, with the identification $a = 2j + 1$.

Numerical Results

In table 5 we give the ground state energy per 2 sites $E_0(M)/M$ ($M = N/2$) of the XXZ model (38), which coincides with the ground state energy per site of the corresponding Potts model. This table should be compared with table 1b in reference [35], which was obtained using the Bethe ansatz. The authors of [35] give their results up to 6 decimals (ours is 9) and the agreement in the energies holds until the 6th digit. The number of states retained in our computation is $m = 160$.

Using the IRF-DMRG data we have computed the finite size corrections to the ground state energy, which are governed by the formula [40, 41],

$$E_0(M)/M = e_\infty + \frac{f_\infty}{M} - \frac{\pi \zeta c}{24M^2} + o(M^{-2}) \quad (48)$$

where e_∞ and f_∞ are, respectively, the bulk and surface energy per site. ζ can be identified with the spin wave velocity and it is given for the Potts model by,

$$\zeta = \frac{\pi \sin \gamma}{2\gamma} \quad (49)$$

We have used Sach's formula to get the values of the central charge c [42].

The outcome of this computation is that the IRF-DMRG method reproduces rather accurately the results obtained using the Bethe ansatz. This supports the hypothesis that the DMRG is in fact an exact numerical RG method.

N/2	r=3 (Q=2)	r=5 (Q=3)	r=7 (Q=3.414)	r=inf (Q=4)
2	-1.320 899 500	-1.478 675 250	-1.537 532 848	-1.616 025 403
4	-1.459 958 153	-1.580 754 400	-1.626 304 313	-1.687 466 299
8	-1.532 472 880	-1.636 075 843	-1.675 237 896	-1.727 934 286
16	-1.569 617 420	-1.665 066 291	-1.701 130 752	-1.749 664 452
32	-1.588 433 915	-1.679 941 590	-1.714 488 941	-1.760 960 537
64	-1.597 906 426	-1.687 482 175	-1.721 280 643	-1.766 733 433
128	-1.602 659 177	-1.691 279 439	-1.724 706 257	-1.769 649 934
256	-1.605 039 733	-1.693 185 000	-1.726 426 767	-1.771 116 470
512	-1.606 231 063	-1.694 139 540	-1.727 288 989	-1.771 851 868
e_∞	-1.607 423 097	-1.695 095 264	-1.728 152 544	-1.772 588 719
(AB ³ Q)	-1.607 423	-1.695 095	-1.728 152	-1.772 588
f_∞	0.610 501 838	0.489 636 433	0.442 486 891	0.377 747 124
(AB ³ Q)	0.610 502	0.489 637	0.442 487	0.377 649
c	0.499 942	0.798 817	0.893 150	1.038 18
(AB ³ Q)	0.500 00(1)	0.799 9(2)	0.89(3)	0.99(2)
(exact)	0.5	0.8	0.892 857	1

Table 5: Ground state energy per 2-sites of the RSOS chain. We also give the results of ref [21] (AB³Q) for e_∞ , f_∞ and c .

V) Vertex-IRF Map

We shall illustrate this map in the case of a spin- s chain whose dynamics is dictated by a rotational invariant Hamiltonian. The Hilbert space of the spin- s chain with N sites will be denoted by $\mathcal{V}^{N,s}$ and consists in the tensor product of N copies of the vector space $V_s = \mathbf{C}^{2s+1}$, where acts the local spin operators \mathbf{S}_i ($i = 1, \dots, N$). The vertex-IRF map is based on the tensor product decomposition of the space $\mathcal{V}^{N,s}$ into its irreducible components.

Vertex Hilbert Spaces \rightarrow IRF Hilbert Spaces

Using the Clebsch-Gordan decomposition of tensor product of irreps of $SU(2)$ one can write,

$$\mathcal{V}^{N,s} = \sum_{0 \leq j \leq 2sN} \mathcal{H}_j^{N,s} \otimes V_j \quad (50)$$

where $\mathcal{H}_j^{N,s}$ is the generalization of the IRF Hilbert space (34) to the spin s case. The heights $a_i \in \frac{1}{2}\mathbf{Z}_+$ that label the IRF states are subject to the following constraints,

$$\begin{aligned} a_0 &= 0 \\ a_1 &= S \\ |S - a_i| &\leq a_{i+1} \leq |S + a_i|, \quad i = 1, \dots, N-1 \\ a_N &= j \end{aligned} \quad (51)$$

The dimension of $\mathcal{H}_j^{N,s}$ is given by the number of times the spin- j irrep appears in the CG-decomposition of the tensor product $s \otimes \dots \otimes s$,

$$\dim \mathcal{H}_j^{N,s} = \text{multiplicity of } V_j \text{ in } \mathcal{V}^{N,s} \quad (52)$$

$\dim \mathcal{H}_j^{N,s}$ can be computed using the following formula,

$$\dim \mathcal{H}_j^{N,s} = \dim \mathcal{V}_j^{N,s} - \dim \mathcal{V}_{j+1}^{N,s} \quad (53)$$

where $\mathcal{V}_{s^z}^{N,s}$ denotes the subspace of $\mathcal{V}^{N,s}$ with a fixed value s^z of the third component of the spin. Eq.(53) says that the highest weights with total spin j are given by the states with spin $s^z = j$ minus the ones that can be obtained from $\mathcal{V}_{s^z+1}^{N,s}$ by the lowering operator S^- . The counting of states with a fixed value of s^z is easily done using the "Bethe method" of starting with the ferromagnetic state with all the spins up and lowering the spin. Below we give the formulae for $s=1/2$ and 1.

$$\begin{aligned} \dim \mathcal{V}_{s^z}^{N,s=1/2} &= \binom{N}{\frac{N}{2} - s^z} \\ \dim \mathcal{V}_{s^z}^{N,s=1} &= \sum_{k=0}^{[(N-s^z)/2]} \binom{N}{s^z + k} \binom{N - s^z - k}{k} \end{aligned} \quad (54)$$

where the symbol $[x]$ appearing in the upper limit of the sum denotes the integer part of x . The relation between the vertex basis of the spaces $\mathcal{V}^{N,s}, V_j$ and the IRF basis of $\mathcal{H}_j^{N,s}$ can be obtained using the Clebsch-Gordan coefficients as follows,

$$\begin{aligned} &\xi(\mathbf{a}) \otimes e_m^j \\ &= \sum_{m_1, \dots, m_N} \begin{bmatrix} 0 & s & a_1 \\ 0 & m_1 & n_1 \end{bmatrix} \begin{bmatrix} a_1 & s & a_2 \\ n_1 & m_2 & n_2 \end{bmatrix} \begin{bmatrix} a_2 & s & a_3 \\ n_2 & m_3 & n_3 \end{bmatrix} \cdots \\ &\cdots \begin{bmatrix} a_{N-2} & s & a_{N-1} \\ a_{N-2} & m_{N-1} & n_{N-1} \end{bmatrix} \begin{bmatrix} a_{N-1} & s & a_N \\ n_{N-1} & m_N & n_N \end{bmatrix} e_{m_1}^s \otimes \cdots \otimes e_{m_N}^s \end{aligned} \quad (55)$$

where $n_i = m_1 + \cdots + m_i$, $m = n_N = \sum_{i=1}^N m_i$, and \mathbf{a} denote the IRF labels which satisfy conditions (51). A graphical representation of eq.(55) is given in Fig.16. The 0 at the upper left of the diagram can be identified with the \star symbol introduced in section II. The vertex-IRF map, as defined by eq.(55), is nothing but a change of basis from vertex variables to IRF ones which achieves the factorization of the $SU(2)$ symmetry.

Vertex-Hamiltonians \rightarrow IRF-Hamiltonians

The most general form of a rotational invariant Hamiltonian H acting in $\mathcal{V}^{N,s}$, i.e.

$$[H, \mathbf{S}] = 0, \quad \mathbf{S} = \sum_{i=1}^N \mathbf{S}_i \quad (56)$$

which is translational invariant and contains only nearest neighbours couplings is given by,

$$H = \sum_{i=1}^{N-1} \sum_{r=0}^{2s} \alpha_r (\mathbf{S}_i \cdot \mathbf{S}_{i+1})^r \quad (57)$$

where α_r is a set of $2s+1$ coupling constants (α_0 can be put equal to zero since it multiplies the identity operator). Since (57) commutes with $SU(2)$ it means that its action affects only the IRF spaces \mathcal{H}_j^N . Using group theoretical methods we get,

$$H \xi(\mathbf{a}) = \sum_{i=1}^{N-1} R \begin{pmatrix} a_{i-1} & a'_i \\ a_i & a_{i+1} \end{pmatrix} \xi(\cdots, a_{i-1}, a'_i, a_{i+1}, \cdots) \quad (58)$$

where the IRF "weights" R can be computed in terms of the coupling constants α_r and the 6j-symbols as follows (the details of this computation will be given elsewhere),

$$R \begin{pmatrix} a_{i-1} & a'_i \\ a_i & a_{i+1} \end{pmatrix} = \sum_{0 \leq j \leq 2s} A_j^{ss} \begin{Bmatrix} s & s & j \\ a_{i-1} & a_{i+1} & a_i \end{Bmatrix} \begin{Bmatrix} s & s & j \\ a_{i-1} & a_{i+1} & a'_i \end{Bmatrix} \quad (59)$$

$$\begin{aligned} A_j^{ss} &= \sum_{r=0}^{2s} \alpha_r x_j^r \\ x_j &= \frac{1}{2}j(j+1) - s(s+1) \end{aligned} \quad (60)$$

As an example we may choose H to be the sum of all the permutation operators between nearest neighbours, in which case A_j^{ss} turns out to be a sign factor,

$$H = \sum_i P_{i,i+1} \implies A_j^{ss} = (-1)^{2s-j} \quad (61)$$

The IRF hamiltonian corresponding to (61) is given by,

$$R \begin{pmatrix} a_{i-1} & a'_i \\ a_i & a_{i+1} \end{pmatrix} = (-1)^{a_{i-1}+a_{i+1}-a_i-a'_i} \begin{Bmatrix} s & a_{i-1} & a_i \\ s & a_{i+1} & a'_i \end{Bmatrix} \quad (62)$$

The $s=1/2$ Heisenberg Hamiltonian (31) is precisely of the form (61) so that table 2 can be derived from (62). In a subsequent publication we shall use eq.(59) to study higher spin Heisenberg chains in the IRF formalism.

Vertex-DMRG \rightarrow IRF-DMRG

The DMRG algorithm to renormalize a block B plus one point \odot into a new block B' , is based on the superblock $B \odot \odot B^R$, where B^R is the reflection of the block B (we use \odot to distinguish vertex-points from IRF-points which were denoted above by \bullet). The main steps of the vertex-DMRG are:

- Diagonalization of the superblock Hamiltonian to find the ground state $|\psi\rangle$.
- Construction of the reduced density matrix by tracing over the states in $\odot B^R$,

$$\rho^{B\odot} = \text{Tr}_{\odot B^R} |\psi_0\rangle\langle\psi_0| \quad (63)$$

- Diagonalization of $\rho^{B\odot}$ to find the eigenvalues w_α and eigenvectors $|u^\alpha\rangle$. Discard all but the largest m eigenvalues and associated eigenvectors.

- Construct the operator T using the truncated eigenvectors $|u^\alpha\rangle$.
- Renormalize all the operators using the analog of eq. (21) in the vertex case.
- Repeat the process for the new block B' .

These set of rules define the vertex-DMRG algorithm, which applies directly to systems where the lattice variables associated to the points \odot are not subject to constraints except perhaps for conservation laws like total spin, charge, etc. Most of the Hamiltonians in Condensed Matter or Stat. Mech. are of this form. If the vertex Hamiltonian happens to have a continuous symmetry, then the factorization of that symmetry would lead naturally to an IRF model, whose renormalization can be studied using the IRF-DMRG method.

The relation between the vertex-DMRG and the IRF-DMRG algorithms, presented in section III, is illustrated diagrammatically in fig.17: the height a (resp. b) labels the different irreps (f.ex. the total spins of the spin chains studied above) that appear in the tensor product of all the irreps contained in the block B (resp. B^R). The intermediate height j is obtained tensoring a (resp. b) with the irrep carried by the vertex \odot , which in the case of the spin chains is a spin- s irrep. Finally, we must tensor $j \otimes j$ and pick up the identity irrep. Let us now find the analytic relation between the vertex and IRF density matrices. We shall call \mathcal{V}^B (resp. \mathcal{V}^{B^R}) the Hilbert space associated to the block B (resp. B^R). The tensor product decomposition (50) becomes in this case

$$\begin{aligned}\mathcal{V}^B &= \sum_a \mathcal{H}_a^B \otimes V_a \\ \mathcal{V}^{B^R} &= \sum_a V_a \otimes \mathcal{H}_a^{B^R}\end{aligned}\tag{64}$$

Using this decomposition the Hilbert space of the superblock $B \odot \odot B^R$ becomes,

$$\mathcal{V}^{B \odot \odot B^R} = \sum_{a,b} \mathcal{H}_a^B \otimes V_a \otimes V_s \otimes V_s \otimes V_b \otimes \mathcal{H}_b^{B^R}\tag{65}$$

The ground state of any rotational invariant Hamiltonian acting in this superblock can be written in the basis of (65) as follows (see fig.18),

$$\begin{aligned}|\psi_0\rangle &= \sum |\xi_a \otimes m_a \otimes m_1 \otimes m_2 \otimes m_b \otimes \eta_b\rangle \psi_{\xi_a, \eta_b}(a, j, b) \\ &\begin{bmatrix} j & j & 0 \\ m_a + m_1 & m_b + m_2 & 0 \end{bmatrix} \begin{bmatrix} a & s & j \\ m_a & m_1 & m_a + m_1 \end{bmatrix} \begin{bmatrix} s & b & j \\ m_2 & m_b & m_2 + m_b \end{bmatrix}\end{aligned}\tag{66}$$

where $\psi_{\xi_a, \eta_b}(a, j, b)$ is the IRF wave function of the ground state $|\psi_0\rangle$.

The density matrix $\rho^{B \odot}$ can be obtained from (63). Using the properties of the CG coefficients we get,

$$\begin{aligned}\rho^{B \odot} &= \sum |\xi_a \otimes m_a \otimes m_1\rangle \langle \xi_{a'} \otimes m'_{a'} \otimes m'_1| \\ &= \frac{\delta_{m_a + m_1, m'_{a'} + m'_1}}{2j+1} \rho_{\xi_a}^{\xi_{a'}} \begin{pmatrix} & a' & \\ * & & b \\ & a & \end{pmatrix} \begin{bmatrix} a & s & j \\ m_a & m_1 & m_a + m_1 \end{bmatrix} \begin{bmatrix} a' & s & j \\ m'_{a'} & m'_1 & m'_{a'} + m'_1 \end{bmatrix}\end{aligned}\tag{67}$$

where

$$\rho_{\xi_a}^{\xi_{a'}} \begin{pmatrix} & a' \\ * & j \\ & a \end{pmatrix} = \sum_{b, \eta_b} \psi_{\xi_a, \eta_b}(a, j, b) \psi_{\xi_{a'}, \eta_b}^*(a', j, b) \quad (68)$$

coincides with the definition of the IRF-DM given in (29). The relation (67) between the vertex and IRF density matrices can be finally written as,

$$\rho^{B\odot} = \sum_j \frac{1}{2j+1} \rho^{S\bullet} \quad (69)$$

The factor $1/(2j+1)$ takes care of the degeneracy of the irrep V_j in the CG decomposition $a \otimes s \rightarrow j$, and guarantees the correct normalization conditions of both density matrices.

VII) Conclusions and Perspectives

We have generalized in this paper the DMRG method to 1d Hamiltonians of IRF type and showed, in the examples of the spin 1/2 SOS and RSOS models, that it gives very accurate results. Our method is equivalent, by means of a vertex-IRF map, to the standard DMRG method formulated by White for Hamiltonians of the vertex type. This map consists in the factorization of the symmetry group of the vertex theory. This factorization has numerical and conceptual advantages. From a numerical point of view one needs to keep a smaller number of states in the IRF-DMRG in order to achieve the same accuracy as in the vertex-DMRG. The degeneracy of the eigenvalues of the vertex formulation, due to the symmetry, is absent in the IRF case, which makes the numerical analysis more compact and stable. Conceptually the IRF-DMRG is also very appealing since it employs tools and techniques well known in Statistical Mechanics, Integrable Systems, Multi-Matrix Algebras and Conformal Field Theory. Thus the IRF states can be seen as paths of a Bratelli diagram, kinks of a Theory of Solitons, discretized strings and conformal blocks in CFT. The formalism we have developed allow us to apply the DMRG method to IRF states in a very natural way.

Let us mention some of the lines of research which we believe deserve further study,

- **Higher Spin and Ferromagnetic Spin Chains:** In section V we have presented the necessary tools to study higher spin chains. A particular interesting case is the spin 1 chain, which has a rich phase diagram. We shall show in a subsequent publication that the string order parameter of den Nijs and Rommelse [43], which is used to characterize the Haldane phase, adopts a particular simple form when written in IRF variables. In fact the IRF states constitute a complete and orthonormal basis of valence bond states. In particular the AKLT state [44], which is a pure Haldane state, is simply a straight path in the Bratelli diagram of the spin 1 Heisenberg chain.

The IRF-DMRG is also very promising for the study of ferromagnetic systems, which seems to display a rich phase structure in the presence of magnetic fields [45]. The vertex-DMRG method applied to ferromagnetic systems encounters the difficulty that the ground state has a huge degeneracy. As we have shown in this paper, the IRF-DMRG eliminates this degeneracy, avoiding the complications arisen from that fact.

- **t-J and Hubbard models:** The vertex-IRF map can be straightforwardly applied to these models yielding an IRF formulation where the spins form valence bonds. The IRF heights are now given by the couple (spin (j), charge (q)). In the case of Hubbard model the symmetry group is given by $SO(4)$ and it contains, in addition to the rotational group, the group of pseudo spin rotations. The factorization of this larger group should reduce considerably the dimension of the Hilbert Spaces.
- **Ladders:** These systems, which have received considerably attention in the last 2 years, consist of a finite number of coupled chains, with very interesting properties (for a review see [46]). For spin ladders with a few number of chains it is rather simple to obtain their IRF version simply by taking the tensor product of the irreps located on the rungs and performing afterwards their tensor product along the chains. This procedure imitates the strong coupling analysis applied to these kind of systems [46]. The IRF models so obtained has more than one link connecting different heights, and so one has to generalize slightly the construction of this paper. A similar multiplicity phenomena occurs in the theory of solitons [47]. The IRF formulation of ladders could be useful to clarify the relationship between their phases and those appearing in higher spin chains.
- **Higher Dimensions** The DMRG philosophy is not confined to 1d, but the standard DMRG algorithms proposed so far are one dimensional, despite of some 2d applications to finite clusters [10]. The IRF-DMRG strengthen this point of view, since in particular the vertex-IRF map is a one-dimensional operation. We should perhaps say that the vertex-IRF map is really adimensional because the tensor product operation does not impose any particular geometry or dimension. In connection with this problem it may be useful to realize that the vertex-IRF map is a duality transformation similar to the Krammers-Wannier duality or the Jordan-Wigner transformation. This interpretation may serve as a guide to construct higher dimensional vertex-IRF maps.

There are still many more topics to be considered in connection with the DMRG. The DMRG method has arisen as a numerical tool specially well adapted to 1d systems, but in our opinion its importance goes beyond its numerical success. There are still some fundamental questions whose solution we would like to know. It is perhaps not exagerrate to say that new and radical developments connected with the DMRG are likely to happen in the near future.

Acknowledgements

We would like to thank Steven White and Miguel A. Martin-Delgado for conversations.

e-mail address: nishino@phys560.phys.kobe-u.ac.jp and sierra@sisifo.ima.iff.csic.es

References

- [1] S.R. White, Phys. Rev. Lett. 69, 2863 (1992); Phys. Rev. B 48, 10345 (1993).
- [2] K. G. Wilson, Rev. Mod. Phys. 47, 773 (1975).
- [3] S.D. Drell, M. Weinstein and S. Yankielowicz, Phys. Rev. D 16, 1769 (1977)
- [4] R. Jullien, P. Pfeuty, J.N. Fields and S. Doniach, Phys. Rev. B 18, 3568 (1978)
- [5] P. Pfeuty, R. Jullien and K.A. Penson, in: Real Space Renormalization, eds. T.W. Burkhardt and J.M.J. van Leeuwen, Series Topics in Current Physics 30, Springer-Verlag, 1982.
- [6] J. Gonzalez, M.A. Martin-Delgado, M.A.H. Vozmediano, Quantum Electron Liquids and High T_c Superconductivity, Lecture Notes in Physics m38, Springer-Verlag 1995. For the RG consult chapter 11.
- [7] S.R. White and D.A. Huse, Phys. Rev. B 48, 3844 (1993)
- [8] E.S. Sorensen and I. Affleck, Phys. Rev. Lett. 71, 1633 (1993); Phys. Rev. B 49, 15771 (1994).
- [9] S.R. White, R.M. Noack and D.J. Scalapino, Phys. Rev. Lett. 73, 886 (1994).
- [10] S.R. White, cond-mat/9604129.
- [11] T. Nishino and K. Okunishi, J. Phys. Soc. Jpn. 65, 891 (1996).
- [12] S. Östlund and S. Rommer, Phys. Rev. Lett. 75, 3537 (1995); cond-mat/9606213.
- [13] T. Xiang, Phys. Rev. 53 , 10445 (1996).
- [14] T. Nishino, J. Phys. Soc. Jpn. 64, 3598 (1995).
- [15] R.J. Bursill, T. Xiang and G.A. Gehring, cond-mat/9609001.
- [16] M.A. Martin-Delgado and G. Sierra, Int. J. Mod. Phys. A 11, 3145 (1996).
- [17] M.A. Martin-Delgado and G. Sierra, Phys. Rev. Lett. 76, 1146 (1996).
- [18] M.A. Martin-Delgado and G. Sierra, Phys. Lett. B 364, 41 (1995).
- [19] M.A. Martin-Delgado, J. Rodriguez-Laguna and G. Sierra, Nucl. Phys. B 473 [FS], 685 (1996).
- [20] R.J. Baxter, "Exactly Solved Models in Statistical Mechanics", Academic Press, London, 1982.
- [21] G.E. Andrews, R.J. Baxter and P.J. Forrester, J. Stat. Phys. 35, 193 (1984).
- [22] E. Date, M.Jimbo, T. Miwa and M.Okado, Phys. Rev. B 35, 2105 (1987).

- [23] F.M. Goodman, P.M. de la Harpe and V. F. R. Jones, "Coxeter-Dynkin Diagrams and Towers of Algebras" , MSRI Publications/Springer-Verlag, New York (1989).
- [24] C. Gomez and G.Sierra, Intern. J. Mod. Phys. A6, 2045 (1991).
- [25] V. Pasquier, Nucl. Phys. B285 [FS19], 162 (1987) ; J. Phys. A 20, L217, L221 (1987).
- [26] E.H.Lieb and F.Y. Wu, in Phase transitions and critical phenomena, vol. I, ed. C. Domb and M.S. Green, Academic Press (1972).
- [27] R.J. Baxter, Ann. Phys. 76, 25 (1973).
- [28] M. Jimbo, T. Miwa and M.Okado, Comm. Math. Phys. 116, 507 (1988).
- [29] V. Pasquier, Comm. Math. Phys. 118, 355 (1988).
- [30] A.A. Belavin, A. M. Polyakov and A.B. Zamolodchikov, Nucl. Phys. B 241, 333, (1984).
- [31] C. Gomez, M. Ruiz-Altaba and G. Sierra, " Quantum Groups in Two Dimensional Physics" , Cambridge University Press, 1996.
- [32] A. Ocneanu, "Quantized groups, string algebras and Galois theory of algebras", London Math. Soc. Lecture Notes 136, 119 (1989).
- [33] A.B. Zamolodchikov and A.Bl. Zamolodchikov, Ann. Phys. 120, 253 (1979).
- [34] S.R. White and R.M. Noack, Phys. Rev. Lett. 68, 3487 (1992).
- [35] F.C. Alcaraz, M.N. Barber and M.T. Batchelor, R.J. Baxter and G.R.W. Quispel, J. Phys. A: Math. Gen. 20, 6397 (1987).
- [36] C.J. Hamer, J. Phys. A: Math Gen, 19, 3335 (1986).
- [37] F.C. Alcaraz, M.N. Barber and M.T. Batchelor, Phys. Rev. Lett. 58, 771 (1987).
- [38] V. Pasquier and H. Saleur, Nucl. Phys. B 330, 523 (1990).
- [39] H.N.V. Temperley and E. Lieb, Proc. Roy. Soc. London A 322, 251 (1971).
- [40] H.W.J. Blote, J.L. Cardy and M.P. Nightingale, Phys. Rev. Lett. 56, 742 (1986).
- [41] I. Affleck, Phys. Rev. Lett. 56, 746 (1986).
- [42] J.M. Van der Broeck and L.W. Schwartz, SIAM J. Math. Anal. 10, 658 (1979).
- [43] M. den Nijs and K. Rommelse, Phys. Rev. B 40, 4709 (1989)
- [44] I. Affleck, T. Kennedy, E. Lieb and H. Tasaki, Commun. Math. Phys. 115, 477 (1988).
- [45] M. Osaka, M. Yamanaka and I. Affleck, cond-mat/9610168.
- [46] E. Dagotto and T.M. Rice, Science 271, 618 (1996).
- [47] C. Gomez and G. Sierra, Nucl. Phys. B 419 [FS], 589 (1994).

Figure Captions

Fig.1.- Bratelli diagram associated to the Coxeter graph A_7 .

Fig.2.- In dark it is shown a path on the Bratelli diagram of Fig.1.

Fig.3.- The string $S_{*,a}$ as a representative of the class of all paths on a Bratelli diagram starting at $*$ and ending at a .

Fig.4.- A string $S_{*,a}$ absorbs a point \bullet which carries an allowed state b , becoming a new string $S'_{*,b}$.

Fig.5.- Diagrammatic representation of the string operators (14).

Fig.6.- Top: diagrammatic representation of the equation (15). Bottom: Diagrammatic reconstruction of the Hamiltonian $H^{S,3\bullet}$.

Fig.7.- Diagrams of the T and T^\dagger operators (17) (T for truncation and for triangle).

Fig.8.- The normalization condition (20) interpreted as a kind of annihilation process of triangles.

Fig.9.- Eq.(23) in pictorial form.

Fig.10.- The renormalization of $\mathcal{O}^{S,2\bullet}$ (see eq.(24)). From figs.8.9 and 10 we see that the RG procedure is a kind of sewing or gluing construction involving triangles, plaquettes and higher n-gons.

Fig.11.- The "super-string" configuration that leads to the infinite system IRF-DMRG algorithm.

Fig.12.- Coxeter graph A_∞ .

Fig.13.- Bratelli diagram built up using the Coxeter graph A_∞ .

Fig.14.- Plot of the deviation of the IRF-DMRG ground state energy of a $s=1/2$ chain with 512 sites, as a function of the number of states retained m .

Fig.15.- Coxeter garph A_r .

Fig.16.- Graphical representation of the vertex-IRF map. Notice that the IRF points \bullet and the vertex points \odot belong to lattices which are dual one another. Indeed the vertex-IRF map is a kind of duality transformation.

Fig.17.- The vertex-IRF map that relates the vertex-DMRG and the IRF-DMRG algorithms.

Fig.18.- Here we show the CG decompositions involved in fig.17.

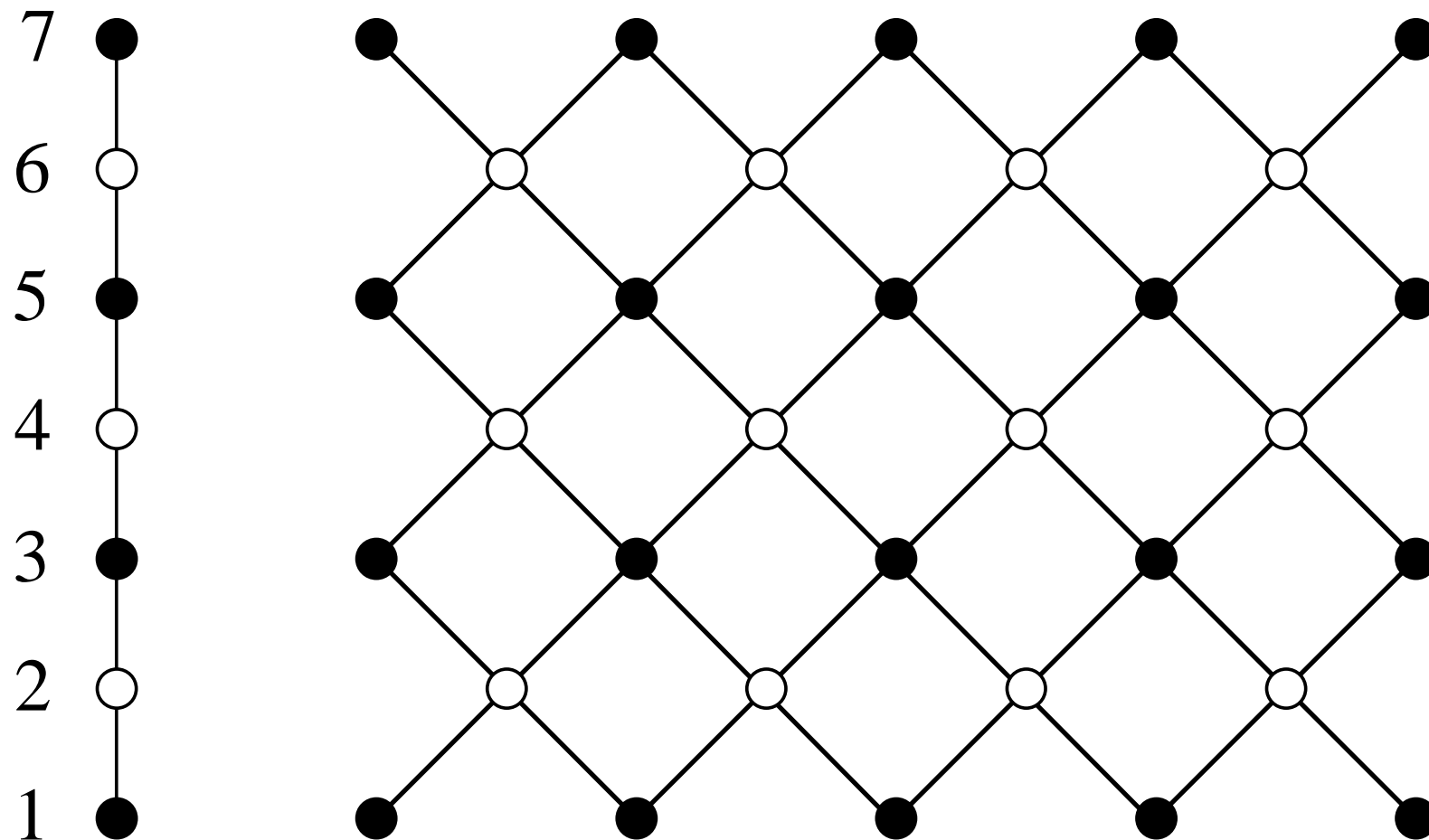


Fig.1

G. Sierra and T. Nishino

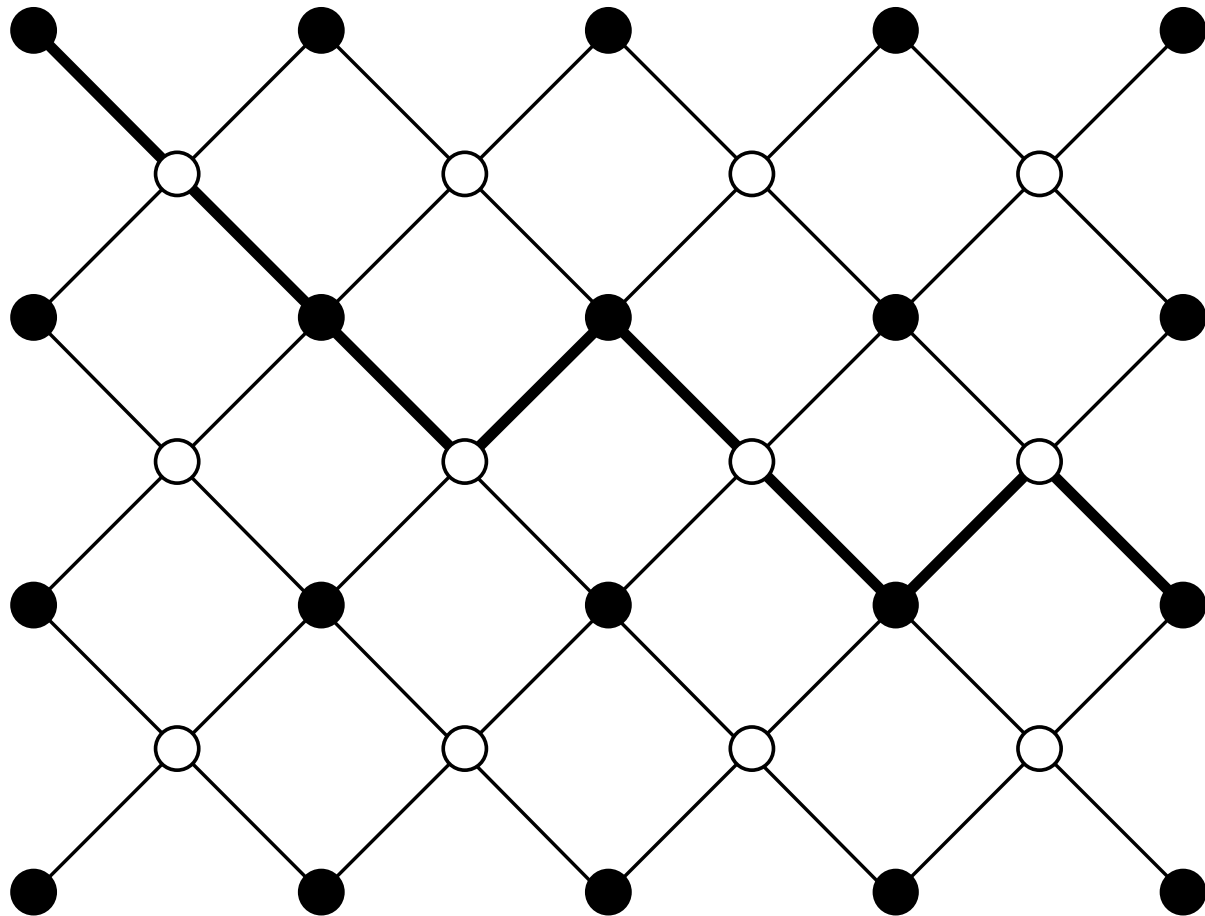


Fig.2

G. Sierra and T. Nishino

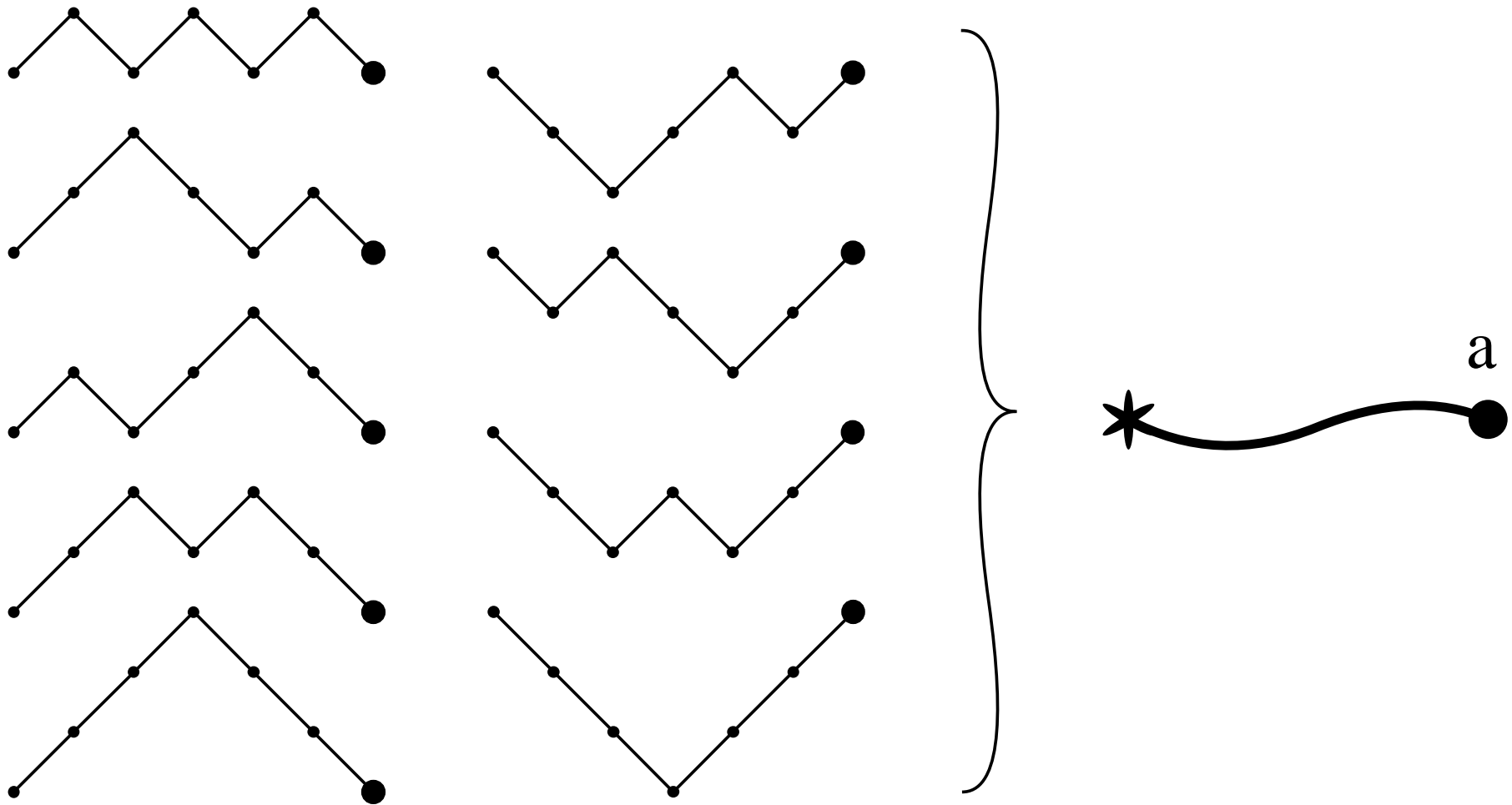


Fig.3
G. Sierra and T. Nishino

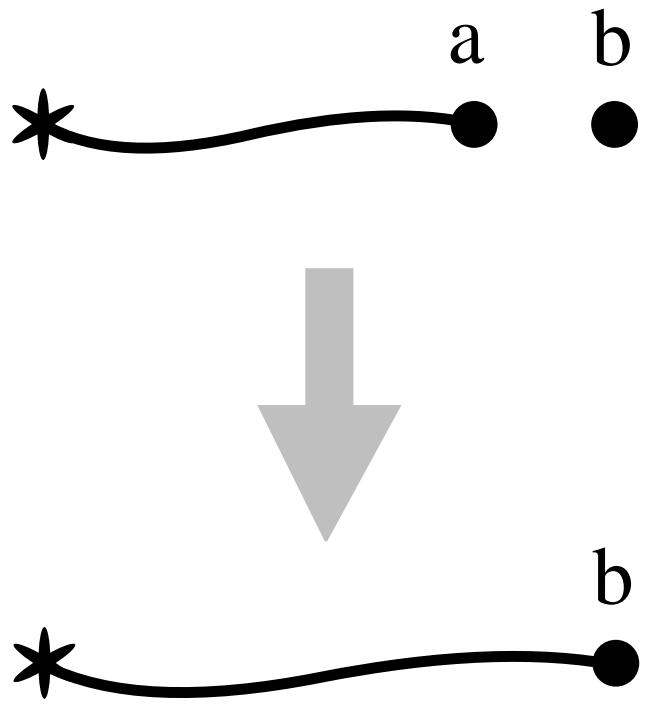


Fig.4
G. Sierra and T. Nishino

$$O_{\mathcal{S}}^{\mathcal{S}'}(*a) = \text{Diagram 1}$$

$$O_{\mathcal{S}}^{\mathcal{S}'}(*\begin{smallmatrix} c \\ a \end{smallmatrix} b) = \text{Diagram 2}$$

$$O_{\mathcal{S}}^{\mathcal{S}'}(*\begin{smallmatrix} e & d \\ a & b \end{smallmatrix} c) = \text{Diagram 3}$$

Fig.5
G. Sierra and T. Nishino

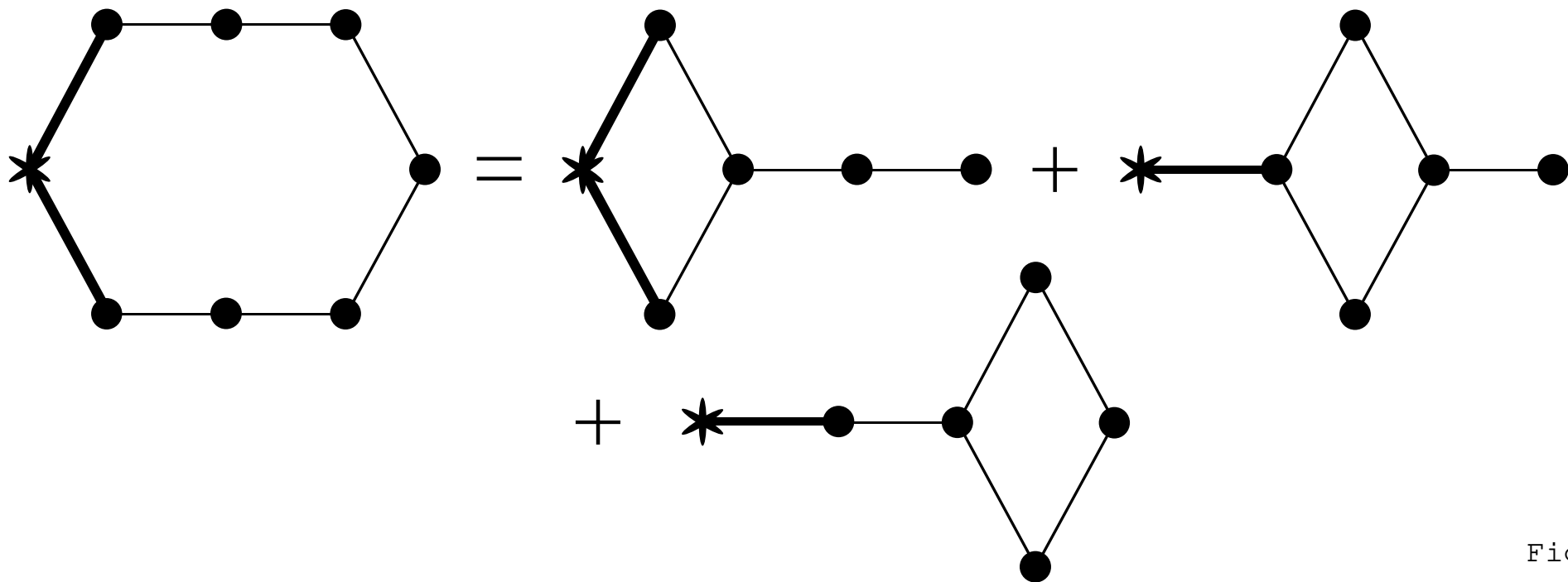
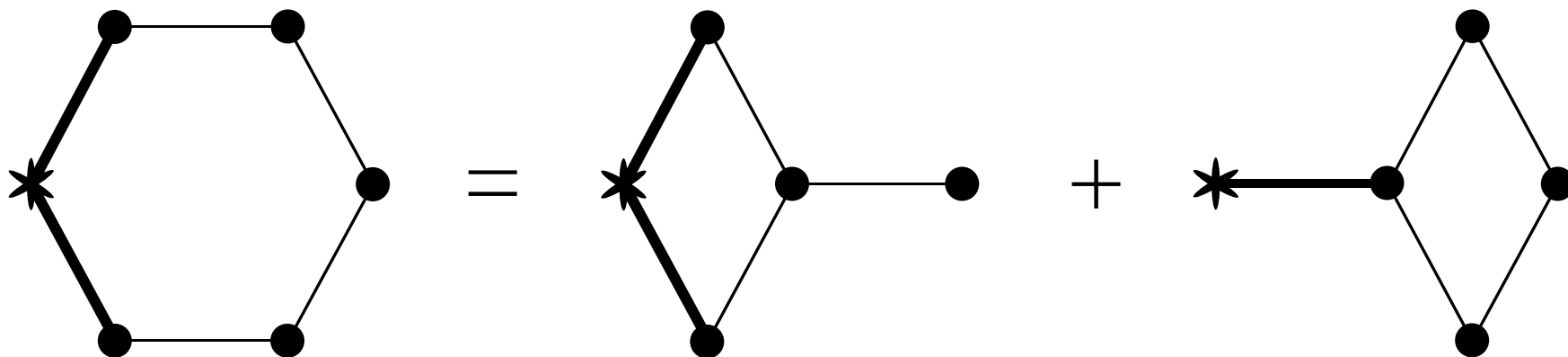


Fig.6
G. Sierra and T. Nishino

$$T_{\zeta}^{\zeta'}(*_a b) = \text{Diagram 1}$$

$$\bar{T}_{\zeta'}^{\zeta}(*^a b) = \text{Diagram 2}$$

Fig.7
G. Sierra and T. Nishino

$$\sum_{a, \zeta} \left[\begin{array}{c} \bullet b \\ \zeta'' \\ \star \\ \zeta \\ \bullet a \\ \zeta' \\ \bullet b \end{array} \right] = \delta_{\zeta' \zeta''}$$

Fig.8

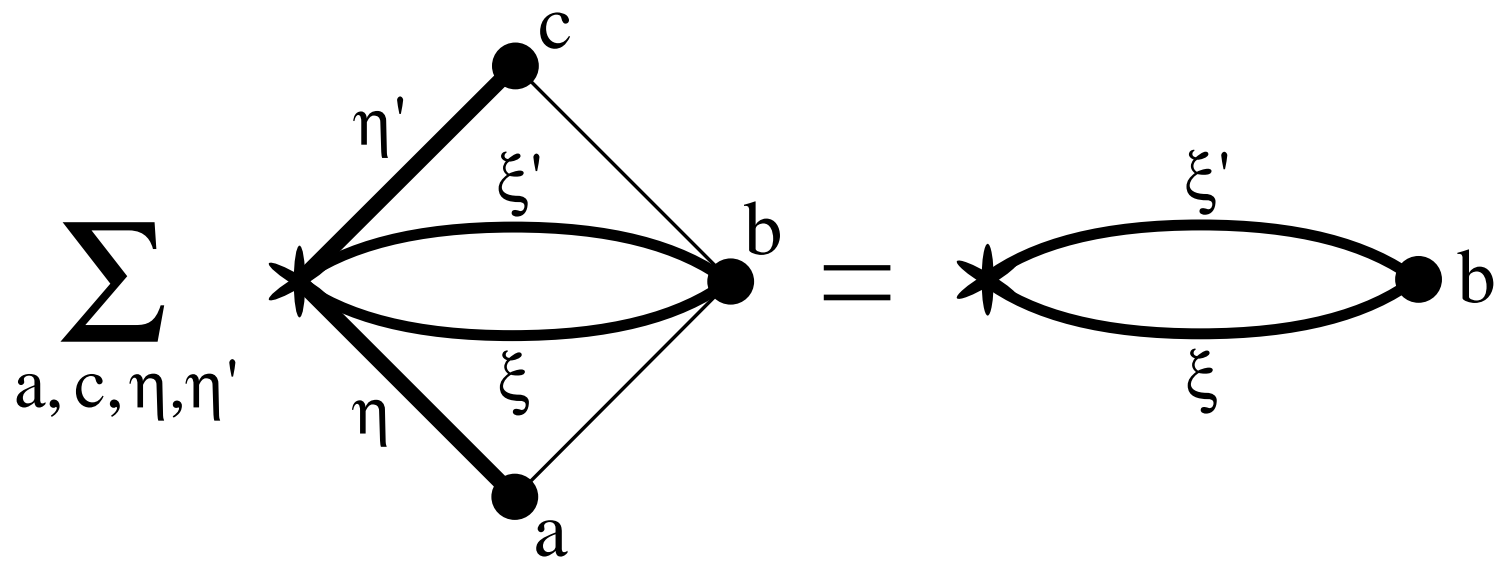


Fig.9

G. Sierra and T. Nishino

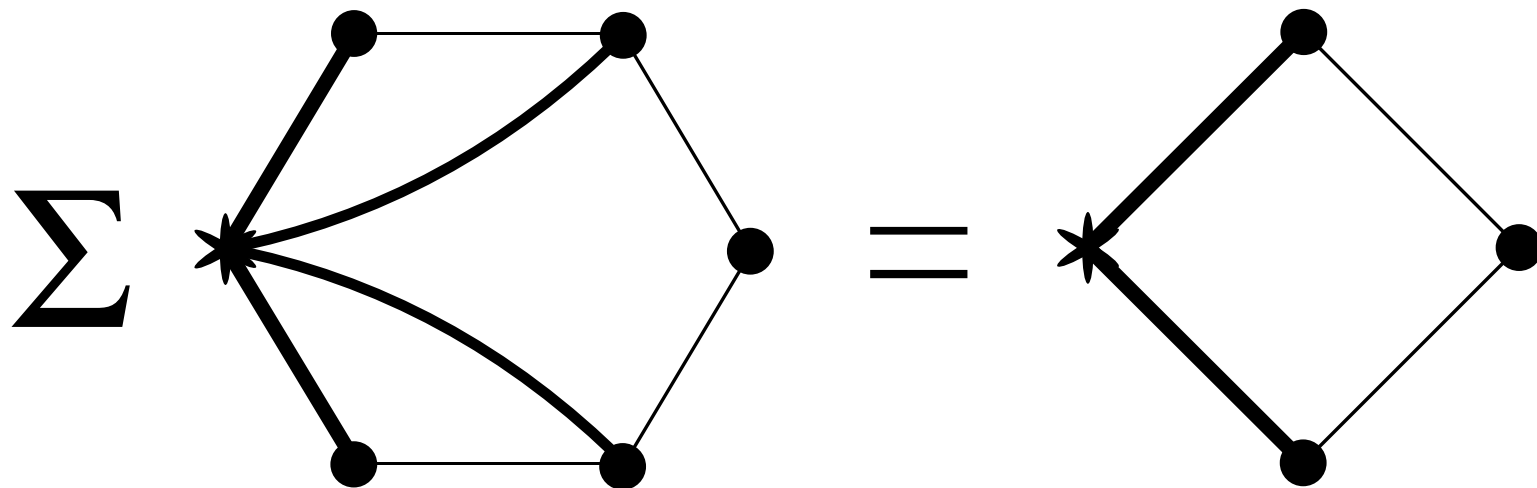


Fig.10

G. Sierra and T. Nishino

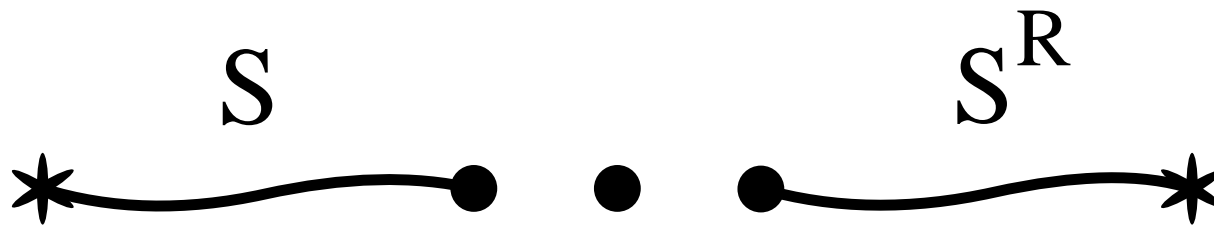


Fig.11

G. Sierra and T. Nishino

$$A_\infty = \begin{array}{ccccccccc} & 0 & 1/2 & 1 & & j-1/2 & j & j+1/2 & \\ & \bullet & \bullet & \bullet & \cdots & \bullet & \bullet & \bullet & \cdots \end{array}$$

Fig.12

G. Sierra and T. Nishino

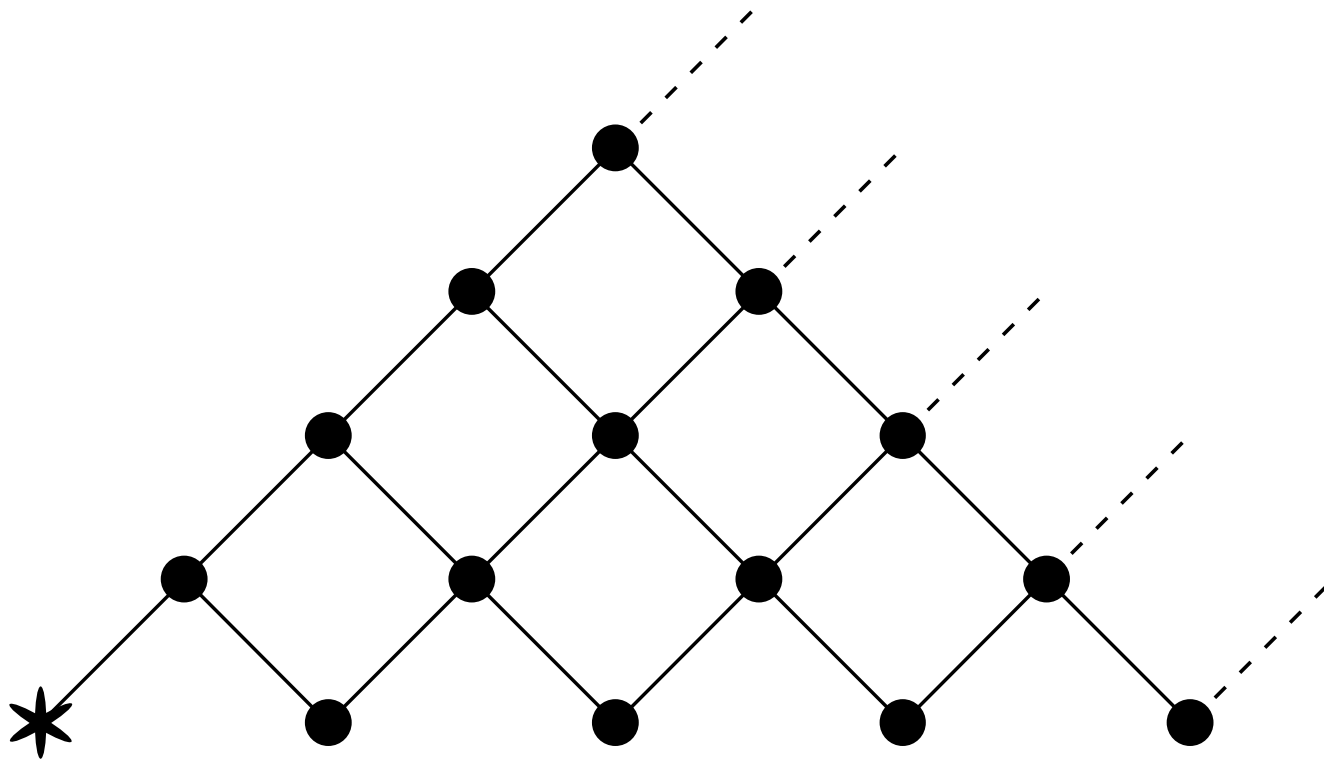


Fig.13

G. Sierra and T. Nishino

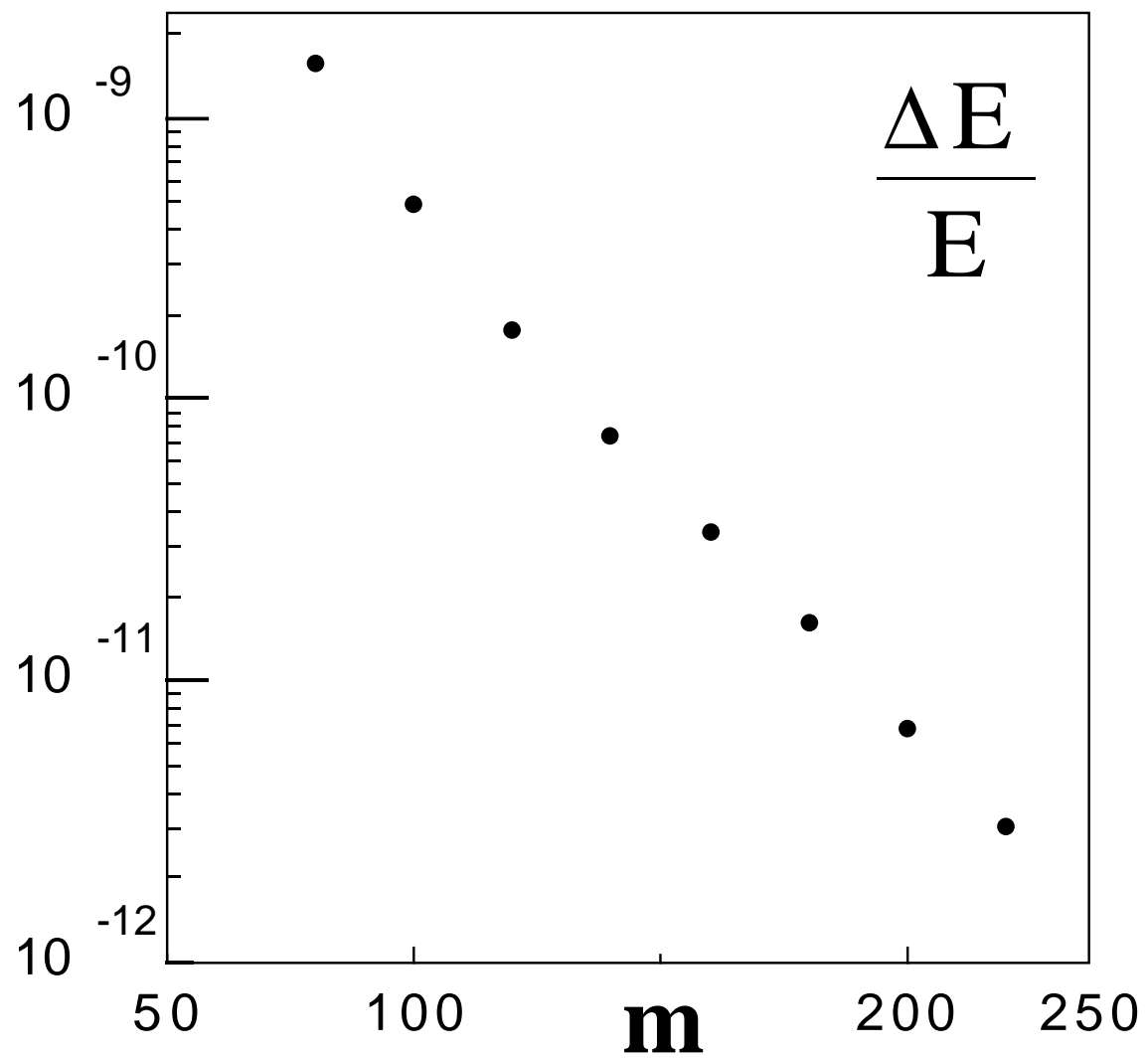


Fig.14

G. Sierra and T. Nishino

$$A_r = \begin{array}{ccccccc} & 0 & 1 & 2 & & r-1 & r \\ & \bullet & \bullet & \bullet & \text{---} & \bullet & \bullet \\ & \text{---} & \text{---} & & & \text{---} & \text{---} \end{array}$$

Fig.15

G. Sierra and T. Nishino

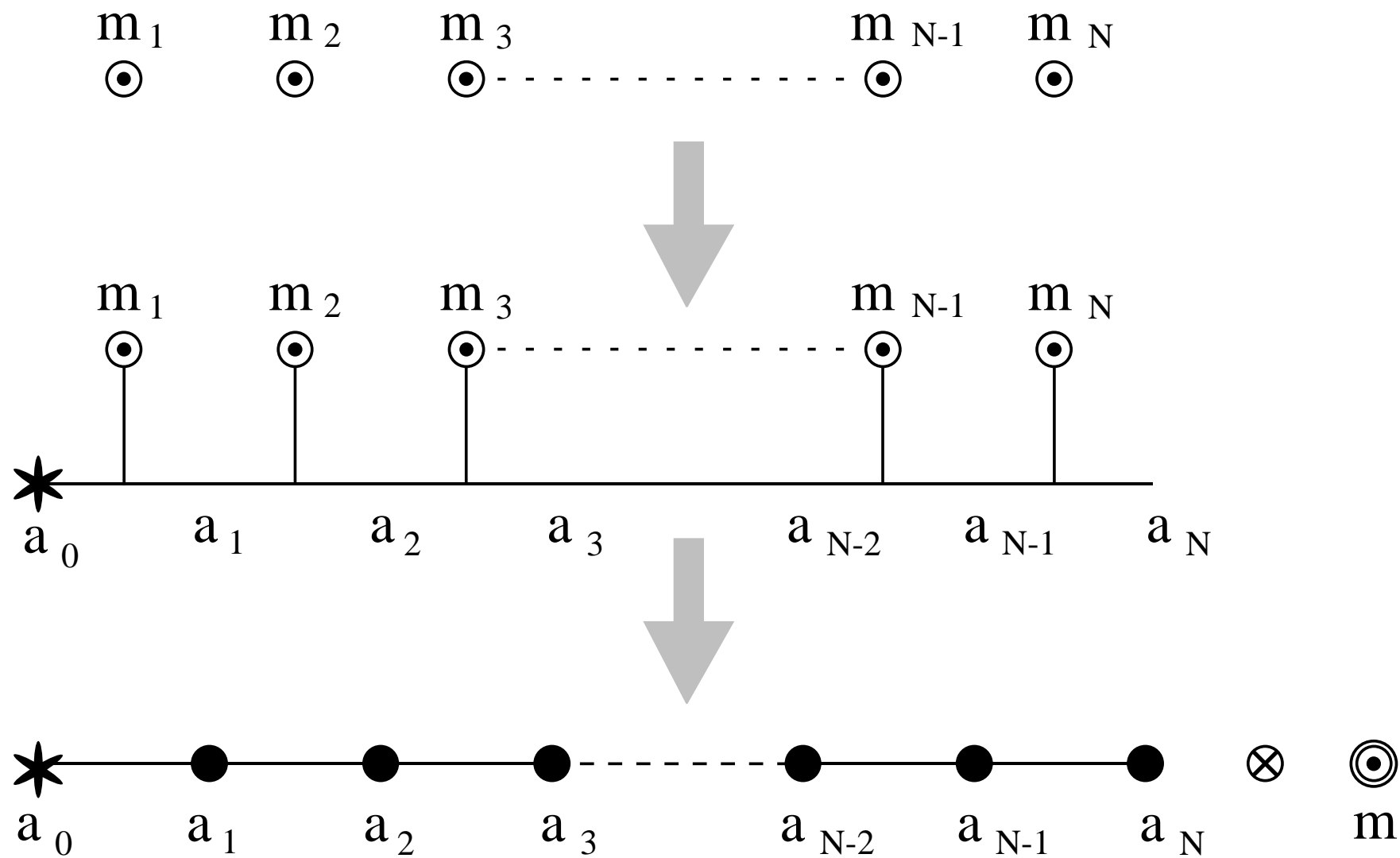


Fig.16
G. Sierra and T. Nishino

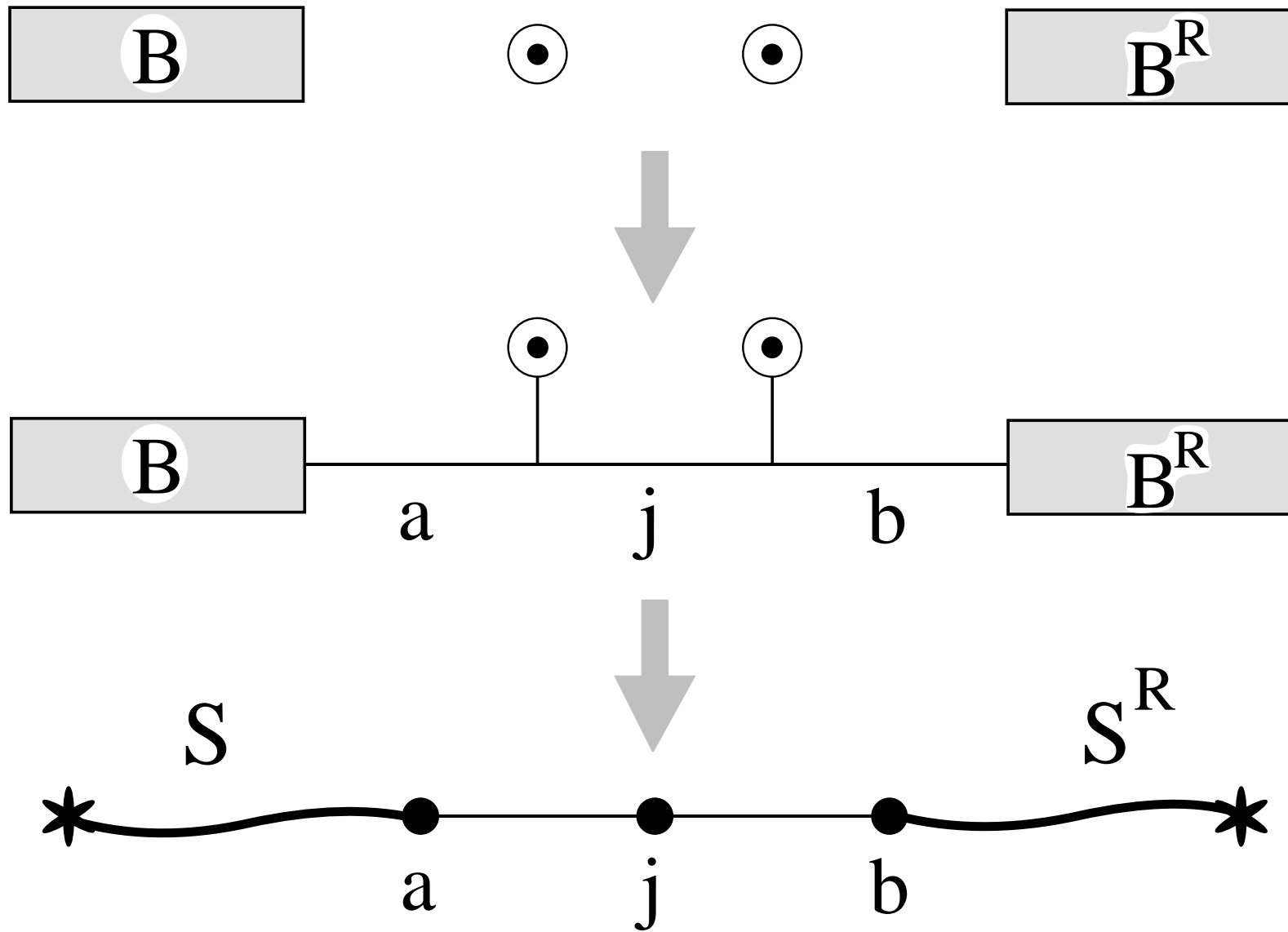


Fig.17

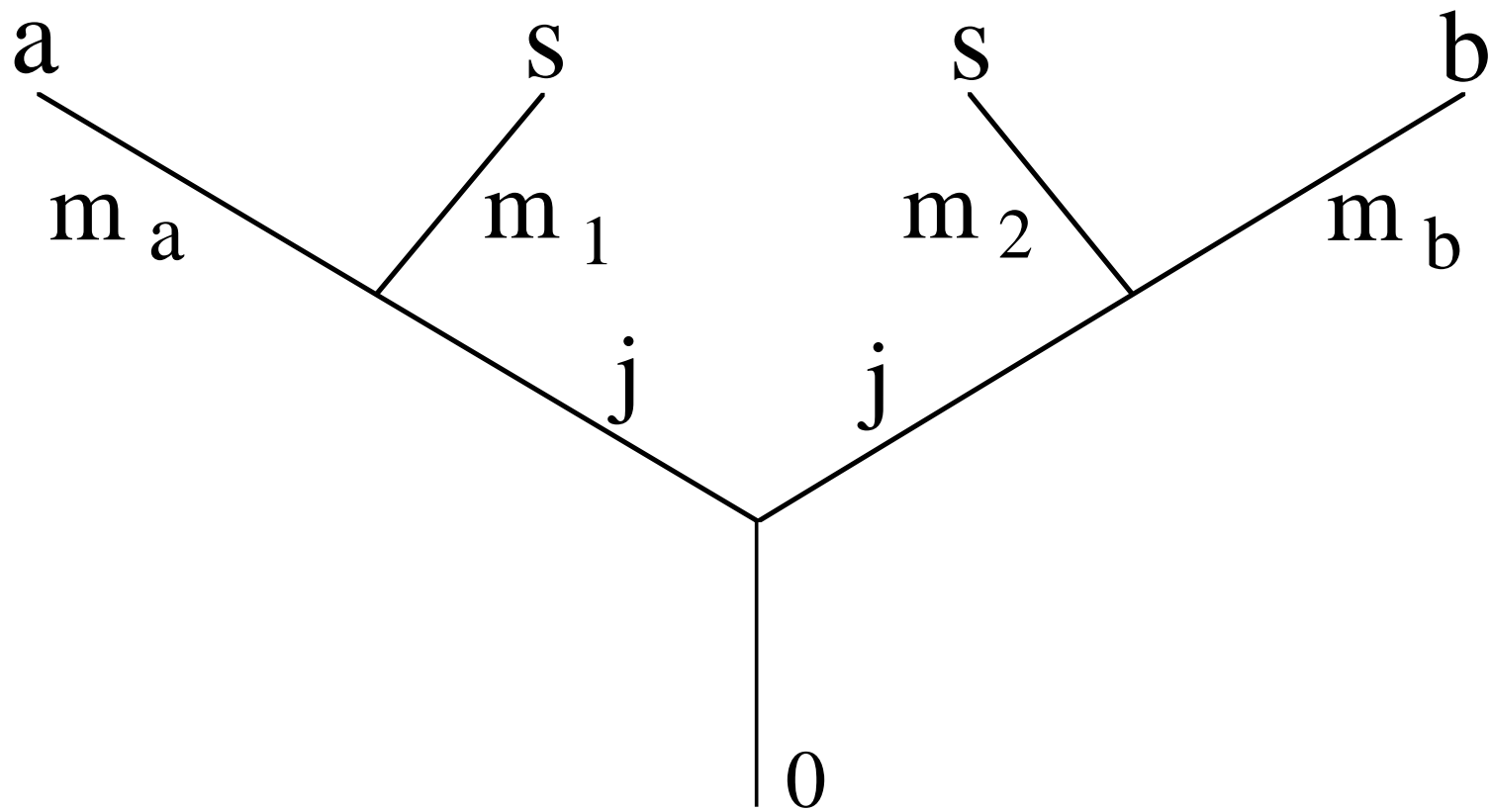


Fig.18

G. Sierra and T. Nishino